The University of Sydney

Department of Civil Engineering
Sydney NSW 2006
AUSTRALIA

http://www.civil.usyd.edu.au/

Centre for Advanced Structural Engineering

Tests of Unstiffened Elements under Combined Compression and Bending

Research Report No R818

Bambach M.R. BE
Rasmussen K.J.R. MScEng, PhD

May 2002

The University of Sydney

Department of Civil Engineering
Centre for Advanced Structural Engineering
http://www.civil.usyd.edu.au/

Tests of Unstiffened Elements under Combined Compression and Bending

Research Report No R818

Bambach M.R. BE
Rasmussen K.J.R. MScEng, PhD

May 2002

Abstract:
Details of a dual-actuator rig developed for testing rectangular plates simply supported on three sides, with the remaining (longitudinal) edge free, under combined uni-axial compression and in-plane bending are presented. Particular attention is given to ensuring a constant strain eccentricity to the loaded ends, as opposed to a constant load eccentricity, in order to determine the post-buckling behavior and ultimate load and moment capacities of unstiffened thin-walled elements. Strain gradients varying from pure compression to pure bending are facilitated. The results of 80 tests on unstiffened plate specimens described herein are used to establish effective width equations for unstiffened elements under stress gradients in a companion report.

Keywords:
Unstiffened plates, stress gradients, plate tests, plate buckling, post-buckling strength, effective widths

Copyright Notice

Department of Civil Engineering, Research Report R818
Tests of Unstiffened Elements under Combined Compression and Bending

mbambach@civil.usyd.edu.au

Published by:
Department of Civil Engineering
The University of Sydney
Sydney NSW 2006
AUSTRALIA

May 2002

http://www.civil.usyd.edu.au

1 INTRODUCTION 5

2 LOAD CASES 5

2.1 LOADING CONDITION – CONSTANT STRAIN ECCENTRICITY 5
2.2 APPLIED STRAIN GRADIENTS 5

3 DUAL-ACTUATOR RIG 6

3.1 GENERAL 6
3.2 PRIMARY ACTUATOR – COMPRESSION RIG 6
3.3 SECONDARY ACTUATOR – BENDING RIG 6
3.4 BOUNDARY CONDITIONS 6
3.5 CONTROL OF THE APPLIED STRAIN GRADIENT 7
3.6 CONTROL LOOP 8
3.7 CONTROL PROCEDURE 8

4 AXIAL DISPLACEMENT MEASUREMENT 9

4.1 GENERAL 9
4.2 STRAIN GAUGE REDUCTIONS 9
4.3 OUTER LVDT REDUCTIONS 10

5 TEST SPECIMENS 10

5.1 PLATE WIDTH 10
5.2 PLATE ASPECT RATIO 11
5.3 PREPARATION 11
5.4 LABELING 11

6 MATERIAL PROPERTIES 11

6.1 COUPON TESTS 11
6.2 COUPON TEST RESULTS 12

7 OUT-OF-PLANE MEASUREMENTS 12

7.1 GENERAL 12
7.2 REDUCTION OF THE OUT-OF-PLANE MEASUREMENTS 12
7.3 GEOMETRIC IMPERFECTION RESULTS 12
7.4 LATERAL DISPLACEMENT PROFILES 12

8 RESIDUAL STRESSES 13

8.1 GENERAL 13
8.2 TENDON FORCE CONCEPT 13
8.3 RESIDUAL STRESS PROFILES IN FLANGE OUTSTANDS 14
8.4 INDUCING EQUIVALENT STRESS PROFILES IN FLANGE OUTSTANDS 14
8.5 WELDING PROCESS 15
8.6 RESULTS OF WELDING PROCESS 15

9 REDUCTION OF FORCE AND MOMENT MEASUREMENTS 16

9.1 TOTAL FORCE 16
9.2 TOTAL MOMENT 16

10 ELASTIC CRITICAL BUCKLING STRESS RESULTS 17

10.1 EXPERIMENTAL ELASTIC BUCKLING STRESS 17
10.2 THEORETICAL ELASTIC BUCKLING STRESS 18
10.3 COMPARISON OF EXPERIMENTAL AND THEORETICAL ELASTIC BUCKLING STRESSES 18
10.4 BUCKLED SHAPES 18
10.5 EFFECTS OF GEOMETRIC IMPERFECTIONS ON BUCKLING 19
10.6 EFFECTS OF RESIDUAL STRESSES ON BUCKLING 19

11 VERIFICATION OF THE RIG 19

11.1 ELASTIC BUCKLING STRESSES 19
11.2 POST-BUCKLING STRENGTH 19

12 ULTIMATE STRENGTH RESULTS 20

12.1 FORCE AND MOMENT VS AXIAL DISPLACEMENT RESULTS 20
12.2 STRESS FROM THE FORCE AND MOMENT VS AXIAL DISPLACEMENT RESULTS 20
12.3 TOTAL STRESS VS AXIAL DISPLACEMENT RESULTS 20
12.4 ULTIMATE CONDITION 20
12.5 ULTIMATE FORCE AND MOMENT RESULTS 21

13 CONCLUSIONS 21

14 REFERENCES 22

15 TABLES 23

16 FIGURES 28

17 APPENDIX A: GEOMETRIC IMPERFECTION PROFILES 43

18 APPENDIX B: LATERAL DISPLACEMENT PROFILES 70

19 APPENDIX C: LOAD vs LATERAL DISPLACEMENT SQUARED CURVES 110

20 APPENDIX D: FORCE AND MOMENT vs AXIAL SHORTENING CURVES 119

21 APPENDIX E: STRESS vs AXIAL SHORTENING CURVES 144

22 APPENDIX F: PHOTOS 164

1 INTRODUCTION

Current specifications for the design of open thin-walled sections provide equations for determining the effective width of stiffened and unstiffened elements, under pure compression and stress gradients. The ultimate capacity of the section is calculated from the effective section properties. Recent studies of cold-formed plain channels by Rasmussen (1994) and fabricated I-sections by Chick and Rasmussen (1999) have demonstrated a marked conservatism in the effective width method when applied to sections containing unstiffened elements under stress gradients. Experimental and analytical results show that beam-column capacities were typically 30% or more higher than those estimated by the current specifications. The conservatism could be traced directly back to the bending capacities, which were of the order of 50% of the actual strengths. Recent studies by Rusch and Lindner (2001) and Beale et al. (2001) have also demonstrated undue conservatism in the effective width provisions for unstiffened elements under stress gradients.

This report outlines an experimental investigation initiated as a means to establishing more accurate design methods for unstiffened elements under stress gradients. In order to determine the fundamental behavior of these elements, the tests were performed on rectangular plates simply supported on three sides, as opposed to testing complete sections, so as to avoid unquantifiable restraints from adjoining elements. Plate tests of this nature have only been reported by Rhodes et al. (1975), where results of 4 tests on individual plates simply supported on three sides are given for varying values of load eccentricity. The loading condition for the experimental investigation presented here is one of constant strain eccentricity.

2 LOAD CASES

2.1 Loading Condition – Constant Strain Eccentricity

The method for the application of the load is critical for unstiffened plate specimens. Researchers testing stiffened plates under stress gradients commonly use rigs that apply a load eccentrically to the ends of the plate, allowing the ends to rotate in-plane to maintain constant loading eccentricity. This method however, does not facilitate accurate results for unstiffened plates. For example, if a load is applied at the centre of an unstiffened plate (zero load eccentricity) (Figure 1a), at elastic local buckling the longitudinal stresses in the plate will redistribute towards the supported edge, and the resistance offered by the plate becomes eccentric (Figure 1b). If the load point remains at the centre of the plate severe in-plane bending is induced, and consequently little post-buckling strength is achieved. This condition is also not congruent to that of plane sections remaining plane in assemblies of plates, which must be satisfied if accurate design methods are to be produced from the tests, since this is the condition of the nodal lines in a member with a number of locally buckled half-wavelengths.

To accurately capture the post-buckling behavior of an unstiffened plate, and maintain a condition of plane sections remaining plane, a rig has been developed that can apply a constant strain eccentricity to the ends of the plate (Figure 2).

2.2 Applied Strain Gradients

The applied strain gradients in the test series consists of those shown in Figure 3. For each of the four load cases, 20 unstiffened plate specimens were tested, over a range of five plate width to thickness ratios.

3 DUAL-ACTUATOR RIG

3.1 General

The rig incorporates the use of two hydraulic actuators, a (primary) 200 ton Dartec actuator applying compressive strains, and a (secondary) 25 ton MTS actuator that is connected to lever arms, applying bending strains to the specimen (Figures 4,5). The dual action can apply strain gradients varying from pure compression to pure bending as required.

3.2 Primary Actuator – Compression Rig

The primary actuator is mounted as a compression rig, with high strength Maccalloy tension bars providing the reaction force to the actuator (Figure 4). The rig is quite flexible compared with those having a fixed reaction frame. As the actuator applies load the tension bars extend elastically, such that the specimen will axially shorten *and* shift in the longitudinal direction.

3.3 Secondary Actuator – Bending Rig

The secondary actuator is seated on support beams and connected to a long square hollow section (SHS in Figure 4). The actuator and the SHS are connected to lever arms that extend to the end platens of the compression rig, where they are rigidly connected. Extension or contraction of the actuator causes the lever arms to rotate about the pin joints shown in Figure 4. The in-plane rotation of the end platens can thus be controlled directly. Since the actuator must move relative to its supports, friction is a concern. To minimise this the actuator is seated on nine ball bearings constrained in a grid, denoted J15 in Figure 4, and the SHS is seated on four ball bearings, such that the lever arm rig is essentially floating.

3.4 Boundary Conditions

Establishing simply supported boundary conditions is essential, particularly for the loaded ends of the plate. The elastic critical buckling stress for slender plates is significantly higher if rotational restraint exists at the simply supported loaded ends. In order to maintain free rotation, the loaded ends of the plate are seated in machined key-ways cut in segments of circular rods, which are fitted into split spherical needle bearings housed in solid bearing blocks, as shown in Figure 6. The rod segments are cut in 20mm lengths, such that the loaded ends of the plate may rotate by varying degrees across the width.

In a slender unstiffened element, the longitudinal stress may redistribute to such an extent after local buckling that tensile stresses may develop at the unsupported edge. If these tensile stresses are not anchored the loaded edge will pull in toward the centre of the plate, and the assumption of plane sections remaining plane will no longer be valid. It is important then to restrain the loaded edge, and for this purpose holes are drilled in the rod segments and in the plate specimens where tensile stresses are likely to occur (Figure 6), and pins are inserted such that the end bearings may resist tension while allowing rotation. This condition is important to the operation of the rig, particularly for the case shown in Figure 3 where compressive strain is applied to the unsupported edge and varies linearly to zero at the supported edge. Slender plates under this load condition have large out-of-plane deflections of the unsupported edge in the post buckling range, and as a result the loaded edges are prone to pulling in.

The pure bending load case, whereby compressive strain is applied to the unsupported edge and tensile strain to the supported edge (Figure 3), presents a unique problem. As the plate is loaded in the post buckling range, the region of the specimen in compression becomes less effective, and a large portion of the

cross-section in tension yields in order to attain ultimate capacity. Drilling holes through the plate to insert pins for resisting tension is not possible, as the plate will fracture through the line of holes and the ultimate condition cannot be captured. For specimens tested under this load condition end plates are welded to the specimen, such that the boundary conditions of the loaded edges are now fixed, not simply supported. As the plates become less effective in the compression zone after buckling occurs, they develop net tension. Stiff compression struts were required between the northern and southern headstocks of the compression rig to facilitate the net tension.

The simple support condition along the unloaded supported edge was achieved by the use of discrete 'finger' supports (Figure 7), which were originally developed at Cambridge University by Moxham (1971). The plate edge is inserted between the first set of pins only and clamped by tightening the top bolt, thus restraining out-of-plane displacements of the edge while allowing rotation. The use of fingers requires no edge preparation to the plate. The fingers are supported on a rod by means of a spherical bearing, such that the fingers may rotate to allow small in-plane transverse displacements of the edge. The rod has a secondary rod beneath it to assist in minimising bending (Figure 4), and both rods are seated in linear bearings. The linear bearings allow the entire finger assembly to shift in the longitudinal direction, in accordance with the shift of the specimen as the tension bars of the compression rig extend. The fingers contain a slender section near the base such that they are flexible in the longitudinal direction, as shown in Figure 7, thus negligible load is transferred through the fingers to the support.

The test setup in Figure 8 shows the use of the end bearings and fingers to provide three sided simple support.

3.5 Control of the Applied Strain Gradient

The flexibility of the rig requires that an independent measurement system be used to control the applied strain gradient. Initially, linear voltage displacement transducers (LVDTs) were mounted on the end bearings on each side of the specimen (Figure 9b), to measure the longitudinal displacement between the end bearings on the east and west sides. However internal displacements within the end bearings preclude accurate measurements of the axial shortening of the plate. The displacements are twofold; firstly there is slack in the bearing between the rod segments and the needle bearing, and within the needle bearing itself, and secondly the bearing block elastically compresses. For the case of uniform compression the slack can be excluded from the results, and experiments have shown this to be of the order of 0.2mm. The compression of the bearing blocks causes a change in slope of the load-displacement curve, or apparent change in stiffness, and this too could be removed from the results with careful processing of the test data. The difficulty arises however with the cases where strain gradients are applied. For these cases the longitudinal edges are compressed by different amounts. The individual rod segments settle by different amounts as the slack is only taken up when load is applied, therefore differential settlement within the bearings occurs across the width of the plate. A measurement system is thus required that can measure the displacement of the loaded ends of the plate directly.

Various displacement measurement systems were investigated, and their accuracy determined by comparison with readings from strain gauges that were fixed to both sides of the plates on each longitudinal edge at mid-length (Figure 8a). The gauges are accurate to within 5 microstrain. The most reliable system was found to be to rigidly attach a rod across the width of the specimen with epoxy glue, as close to the ends as is practical (Figure 9a). LVDTs were mounted on each side of the plate running longitudinally, such that the displacement of the east and west sides was known (Figure 9c). The ratio of the values prescribed the strain gradient on the plate. This method was found to be inaccurate for the more slender specimens however, due to large out-of-plane displacements of the unsupported edge of the plate, causing the rod ends

to displace vertically. For slender specimens, targets were mounted on the rods and laser measurement devices were positioned at each rod end (Figure 8b). The mounting arrangement used bearings to ensure verticality of the target at all stages of plate deflections. The difference between the two readings on each side of the plate gives the displacements of the east and west sides respectively, and the strain gradient may be deduced. If the targets were set carefully only small inaccuracies occurred when the rod ends displaced vertically (i.e. when large lateral displacements occurred). Additional transducers were mounted on the end bearings in all tests, designated "Outer LVDTs" in Figure 10. Figure 10a shows a typical test setup for stocky specimens, and Figure 10b a typical test setup for slender specimens.

In all tests, the strain gauges were used to determine the applied strain gradient until out-of-plane deflections occurred. The gauge readings were not applicable in determining the (average) applied strain after local buckling, since they recorded the localised strain at the centre and did not account for shortening resulting from plate deflections.

3.6 Control Loop

The tests were performed by setting stroke speeds on the digital controllers. The controller for each actuator was set to a prescribed control-slave system according to the strain gradient required, whereby one actuator ran at a set stroke speed, and the other actuator ran as a slave at a ratio of that stroke speed. This was achieved by sending the voltage signal from the internal LVDT of the master actuator to the controller for the slave actuator, and amplifying or reducing the signal accordingly. Due to the flexibility of the rig, the stroke ratio was determined experimentally and needed to be manually adjusted continuously throughout the test. Continuous monitoring of the displacement measurement system allowed the strain gradient to be known at all times during the test, and the stroke ratio was adjusted to maintain the required gradient.

3.7 Control Procedure

The control procedure during a test consisted of monitoring the various measurement devices at different stages of the test, and calculating the ratio of the displacement of the east and west sides. Continuous monitoring was achieved with the use of a data logger, recording and displaying (on a monitor) readings from the measurement devices every 10 seconds. A typical compression test or combined compression and bending test was conducted as follows:

- Strain gauges were used until lateral deflections occurred, signified by the deviation of the magnitudes of the top and bottom surface strain gauges. While the specimen remains straight, the top and bottom strain gauges record strains approximately equal in magnitude, and opposite in sign. A lateral deflection of 1mm will typically incur a difference of 100με between the strain gauges at the deflected edge. This point was nominally taken as the completion point of the use of the strain gauges.
- Longitudinal transducers (stocky specimens) or laser devices (slender specimens) were used until inaccuracies were detected. Inaccuracies in the transducers were signified by a decrease in magnitude, particularly at the unsupported edge, caused by large lateral deflections of the rod ends. Inaccuracies in the laser devices were error values caused by the laser not receiving the return signal from the target. This generally occurred at the unsupported edge where large lateral deflections caused the target to move (vertically) out of range of the laser beam. The targets had a vertical dimension of 40mm, however the laser beam needed to be set at the centre-height such that a vertical range of 20mm could be achieved, regardless of whether the plate buckled up or down. Error messages were thus encountered when the lateral displacement of the unsupported edge reached approximately 20mm.

- Outer LVDTs were used until completion of the test. By this point in the test the axial displacement is relatively large, and settling of the end bearings has already occurred, such that the strain gradient measured from the outer LVDTs is sufficiently accurate.

Completion of the test was deemed to be at a load corresponding to approximately 80% of the ultimate load, in the post-ultimate region, for the pure compression tests. Since the ultimate condition for the combined compression and bending tests was not clearly defined prior to processing of the results (see Section 12.4), these tests were continued as far as possible, the limiting condition being contact between the plate specimen and the end bearing due to large end rotations (Figure 11). A typical test was conducted over a period of one hour.

The pure bending tests used welded end plates, not end bearings, and therefore did not require the rod rigidly attached to the specimen. In these tests, outer LVDTs were mounted on the loading platens. A typical bending test was as follows:

- Strain gauges were used until the outer LVDTs were verified as accurate (compared with the strain gauges), which occurred at very low loads, well before buckling
- Outer LVDTs were used until completion of the test

For the pure bending tests, the limiting condition was the stroke of the secondary actuator, and the tests were continued until the secondary actuator was fully contracted.

4 AXIAL DISPLACEMENT MEASUREMENT

4.1 General

As detailed in Section 3, a number of different measurement devices were used in the tests to determine the applied strain gradient, depending on the loading condition and the slenderness of the specimen (which determines the magnitude of lateral displacements). The values recorded from the various devices must be reduced to produce the axial shortening of the specimen, for plotting against the force and moment values. For the load cases of pure compression and compressive strain at the supported edge and zero at the unsupported edge, all strain gauges were used until a lateral deflection of 1mm was recorded, and thereafter the strain gauges at the supported edge were used, to calculate the axial shortening. The values from the strain gauges at the supported edge are valid throughout the entire test, due to the fact that the lateral deflections at this position are negligible. For the case of compressive strain at the supported edge and zero strain at the unsupported edge, all strain gauges were used until a lateral deflection of 1mm was recorded, and thereafter the outer LVDTs were used to calculate the axial shortening. The outer LVDTs were found to be sufficiently accurate for all specimens under this load case, since the nature of the load case is such that the magnitude of lateral displacements were relatively small. For the case of pure bending, the outer LVDTs are used for the full range. The methods for reducing the recorded data to axial shortening values are presented below.

4.2 Strain Gauge Reductions

Since the fingers needed to be attached along the supported edge, the strain gauges could not be fixed at the edge. For plate specimens of width less than 100mm, the gauges were fixed 10mm in from the longitudinal edges. For those specimens of width greater than 100mm, the gauges were fixed 15mm in from the longitudinal edges. To calculate the strain along a longitudinal edge, the topside and bottomside readings

were first averaged. For the case of pure compression, the average strain at the supported edge is the axial strain in the specimen. For strain gradients, the average is then multiplied by a geometric factor. The geometric factor is based on the strain gradient applied, and is a ratio of the distance the gauge is from the point of zero strain, to the plate width. The factor is used to extrapolate the strain to the edge of the specimen, since the gauges are not positioned at the edge. The edge strain is then multiplied by the specimen length to obtain the axial shortening along the longitudinal edge.

4.3 Outer LVDT Reductions

Compression tests were performed on a single end bearing, with a section of 6mm thick plate of width equal to that of the bearing (nominally 60mm). After a load of approximately 15kN, the slack in the needle bearing is taken up, and the bearing has an average constant compression ratio of 0.005mm/kN. The outer LVDTs are positioned at a distance from the longitudinal edges of the plate (Figure 10), therefore the readings are first multiplied by a geometric factor. The geometric factor is based on the strain gradient applied, and is a ratio of the plate width to the distance the transducer is from the point of zero strain. From these readings the axial shortening of the bearings is deducted, in order to obtain the axial shortening of the plate specimen only. For every reading, the average constant compression ratio of a bearing (0.005mm/kN) was multiplied by the current compression load and then subtracted from the current outer LVDT reading to give the current axial shortening, for the load case of compressive strain at the supported edge and zero strain at the unsupported edge.

For the pure bending specimens, the outer LVDTs were mounted on the loading platens, since end bearings were not used. A geometric factor is introduced in the same way as above, to extrapolate for the axial shortening at the longitudinal edge, since the transducers are at a distance from the specimen edge.

5 TEST SPECIMENS

5.1 Plate Width

The most convenient form of presenting plate test results is in the form of strength curves, where the ultimate stress is normalised with the yield stress, and plotted against the non-dimensionalised slenderness ratio. The slenderness ratio is given by Equation 1, where f_y is the yield stress and f_{cr} the elastic critical buckling stress given by Equation 2, where t is the plate thickness, b is the plate width and k is the elastic buckling coefficient for a particular strain gradient. A range of slenderness values are required between zero and three to provide sufficient data to produce a strength curve. The five nominal values of slenderness ratio chosen are shown in Table 1. A nominal thickness of plate specimen was chosen as 5mm, and was constant for all plate tests, and the plate testing rig was designed for this thickness. The slenderness ratios were thus achieved by varying the plate width. The buckling coefficients (k) were determined using the Finite Strip program THINWALL developed by Papangelis and Hancock (1995), for the load cases being studied (Table 1). The values are for very long plates (of the order of 100 times the width), such that the asymptotic value of the buckling coefficient is used, as given in Bulson (1970). The values compare well with the theoretical solutions by Bulson. The nominal plate widths required to achieve the nominal slenderness ratios are shown in Table 1, and have been rounded to the nearest 5mm. The plate widths for the load case of pure bending with tension at the unsupported edge (designated load case c-2 in Table 1), are large due to the large value of the buckling coefficient of 24.2. Due to the impracticalities of testing plates of this size, this load case was omitted from the test series.

$$\lambda = \sqrt{\frac{f_y}{f_{cr}}} \tag{1}$$

$$f_{cr} = \frac{k\pi^2 E}{12(1-\upsilon^2)\left(\frac{b}{t}\right)^2} \tag{2}$$

5.2 Plate Aspect Ratio

The aspect ratio is defined as the ratio of the plate length to plate width. Stiffened single plates buckle elastically with half-wavelengths equal to the plate width i.e. a square stiffened plate buckles in exactly one half-wave, a stiffened plate with an aspect ratio of two buckles in two half-waves, and so on. An unstiffened plate however, always buckles in a single half-wave when simply supported along the supported longitudinal edge, regardless of the aspect ratio. The value for the aspect ratio was chosen with consideration of the elastic buckling coefficient, and requiring a length sufficient such that end effects are minimised. An aspect ratio of five was used for all specimens, such that the buckling coefficient is within 10% of the asymptotic value in Table 1.

5.3 Preparation

Eighty plates were guillotined from two sheets of mild steel of nominal thickness 5mm, to the nominal plate width dimensions given in Table 1. The lengths were nominally five times the width. The design of the plate testing rig was such that no edge preparation was required. Four specimens of each nominal width were cut for each load case, two of which were subsequently treated with a welding process described in Section 8, such that they contained residual stresses.

5.4 Labeling

The test specimens are labeled according to the load case, plate width and welded condition. The prefix is the load case and corresponds to the abbreviations of c0, c1, c2, c3 in Table 1. The suffix is the nominal plate width and the specimen number, where 1 and 2 designate unwelded specimens, and w1 and w2 designate welded specimens. Figure 12 represents the labeling system diagrammatically. For example a label of c0801 designates a nominal plate width of 80mm, unwelded specimen number one, tested in pure compression, and c080w1 designates a nominal plate width of 80mm, welded specimen number one, tested in pure compression.

6 MATERIAL PROPERTIES

6.1 Coupon Tests

All specimens were cut from one of two sheets of Grade 300 mild carbon steel, with a nominal yield stress of 300MPa. The material properties were determined from tensile tests of coupons cut from each of the two sheets, cut in the longitudinal direction of roll in the manufacturing process. The coupon dimensions conformed to the Australian Standard AS 1391 (1991) for the tensile testing of metals using 12.5mm wide coupons of gauge length 50mm. The coupons were tested according to the Standard AS1391 in an Instron TT-KM (250kN capacity) displacement controlled testing machine using friction grips to apply loading. An extensometer of gauge length 50mm was used to measure the longitudinal strain. A data acquisition system

was used to record the load and the readings of strain at regular intervals during the tests. The static load was obtained by pausing the applied straining for one minute near the 0.2% tensile proof stress and the ultimate tensile strength.

6.2 Coupon Test Results

The material properties determined from the tensile coupon tests are summarised in Table 2. Table 2 contains the nominal 0.2% tensile proof stress ($\sigma_{0.2}$), the measured static 0.2% tensile proof stress ($\sigma_{0.2}$), the tensile strength (σ_u), and the Youngs Modulus (E) and elongation after fracture (ε_u) based on the gauge length of the extensometer (50mm).

The stress-strain curves obtained from the coupon tests are shown in Figures 13-16. In the figures the stress (σ) is the measured load divided by the measured initial cross-section area of the coupon, and the strain (ε) is the extensometer readings divided by the extensometer gauge length.

7 OUT-OF-PLANE MEASUREMENTS

7.1 General

A measurement frame was situated above the specimen (Figures 4,5), and had two high-precision rails running longitudinally. A trolley was mounted by means of linear bearings on the rails, and was attached to a timing belt and pre-programmed stepper motor. Transducers were mounted from the trolley and positioned in a line across the width of the specimen. The line of transducers was run along the length of the specimen before and during the test, and readings were taken every 25mm, producing a fine representation of the initial imperfections and buckled shape.

7.2 Reduction of the Out-of-plane Measurements

The transducers could not record values right to the end of the specimens, due to the presence of the end bearings. Consequently, the imperfections in the region of approximately 30mm from the loaded ends were obtained by linearly extrapolating the measured shape to these intervals. The lateral deflections (under loading) were not deduced in this interval, producing a gap in the deflected shape between the last reading at each end, and the loaded edge.

7.3 Geometric Imperfection Results

The geometric imperfection results are summarised for all specimens in Table 3. For each plate size, the table shows the average of the maximum imperfections at the unsupported edges of the four plates of this size. The average maximum imperfection of the unsupported edge for all specimens is 0.876mm, which corresponds to an imperfection to thickness (t) ratio of 0.175t. Imperfection plots are presented in Appendix A for all specimens. The zero level was determined by fitting a straight line through the end point readings and reducing all readings between the ends relative to this line.

7.4 Lateral Displacement Profiles

Lateral displacement profiles are presented for all specimens in Appendix B. The results are discussed further in Section 10.4.

8 RESIDUAL STRESSES

8.1 General

It is well known that residual stresses are induced in members as a result of welding and flame cutting processes, and that these stresses may influence the load carrying capacity of thin-walled members, particularly those that contain slender component plates. In the 1970s an extensive program was undertaken at Cambridge University to investigate the nature and magnitude of residual stress profiles induced by a large variety of welding processes common to the fabrication of thin-walled steel members. Reports by Kamtekar (1974) and White (1977a) and b) and c) give details of welding experiments performed on single plates and sections, and propose equations that predict the profiles and magnitudes of residual stresses. Reports by Moxham (1971), Dwight and Moxham (1971) and Bradfield (1979) detail welding processes on single plates, for the purpose of inducing residual stresses in plate specimens that were subsequently tested in plate testing rigs. The results of these tests provided valuable data on the effect of residual stresses on the load carrying capacity of stiffened plate elements (plates simply supported on all sides).

8.2 Tendon Force Concept

8.2.1 Centre Welded Plate

The research at Cambridge led to the 'tendon force' concept for bead-on-thin-plate weld shrinkage, whereby a weld may be considered as a tendon exerting a force *F*, which is resisted by the full cross-section. If a continuous weld is laid longitudinally on a thin plate along its centreline, a longitudinal stress pattern is induced that consists of a region of tensile yield stress in the immediate vicinity of the weld, and compressive stress elsewhere, the resultant of which resists the tendon force. For all practical welding and plate parameters, the magnitude of the tendon force is given by White (1977a):

$$F_{centre} = 0.2p\left(\frac{Q}{v}\right) \tag{3}$$

where p is the process efficiency and (Q/v) is the heat input per unit length of weld. The process efficiency for a centre weld was found to be 0.8, and the tendon force was shown to be insensitive to plate width and yield stress. This condition is applicable to the weld shrinkage induced in a flange plate when it is welded into an I-section or T-section. The distribution of longitudinal residual stress is shown in Figure 17a. A small gradient may exist in the compressive zone due to 'wrap up', where small angular distortions may occur about the line of the weld (Figure 17a). It is noted that transverse residual stresses were found to be negligible.

8.2.2 Edge Welded Plate

If the weld is laid eccentrically to the centroid of a plate, a bending stress is induced due to the offset of the tendon force. This causes a stress gradient and increases the magnitude of the tendon force (White (1977b), such that for edge welds it is given by:

$$F_{edge} = 0.32p\left(\frac{Q}{v}\right) \tag{4}$$

The process efficiency (p) was found to be less than that for a centre weld, due to increased heat loss from the weld. White (1977b) suggested a value of 0.42. This condition is applicable to the web in a welded T-section or the flange of a welded channel section. The residual stress gradient generally causes the unwelded edge to be in tension (Figure 17b).

8.2.3 Both Edges Welded Simultaneously

If welds are laid symmetrically and simultaneously, the eccentricities of the tendon forces effectively cancel each other out, and constant compressive stress is induced in the central region of the plate (Figure 17c).

The magnitude of the tendon force is the same as that given for the centre welded plate in Equation 3. This condition is applicable to the web in a welded I-section, when the edges are welded simultaneously, such as in an automatic welding process.

8.2.4 Consecutive Edge Welds

If one edge of the plate is welded and the specimen allowed to cool, the residual stress pattern for a single edge weld is induced (Figure 17b). If the other edge is then welded, this weld is laid in a region of existing tensile stress. Weld theory by White (1977a) shows that the material around the weld yields in compression during the heating cycle before tensile stresses develop at the weld during the cooling process. Laying a weld in a tensile zone results in a reduced width of material yielding in compression during the heating cycle, and the tendon force produced is less than that for a similar weld laid in stress free material. The converse is true for welds laid in regions of compressive stress. Experiments by White (1977b) showed the magnitude of the tendon force to be the same as that for edge welds (Equation 4), but scaled up or down by a factor (m) according to the magnitude of the existing compressive or tensile stresses respectively:

$$F' = m0.32\, p\left(\frac{Q}{v}\right) \tag{5}$$

If edge welds are laid consecutively then, with the same heat input per unit length, and weld 1 inducing tension at the opposite edge, weld 2 will produce a smaller tendon force than weld 1. The residual compressive stress resisting the tendon force will thus be less (Figure 18a). The addition of the residual stresses from each weld produces the final stress profile shown in Figure 18b.

8.3 Residual Stress Profiles in Flange Outstands

Two conditions common to the fabrication of I-sections are detailed here, for the purpose of determining the residual stress profiles existing in flange outstands of fabricated sections. Firstly an I-section fabricated from as-rolled or cold-cut plates, and secondly one fabricated from flame cut plates. In the first case, it may be assumed that the plates are stress free when they are welded to form the section, such that the two flange plates develop a residual stress pattern similar to Figure 17a, and the web similar to Figure 17c. It is assumed that the welding process is automated, such that the welds are laid simultaneously. An I-section fabricated in this way by Chick and Rasmussen (1999) produced the profile shown in Figure 19a, having a nearly uniform compressive stress with an average of 109MPa in the web, and a small gradient in the flanges, where the average compressive stress is also 109MPa.

I-sections that are fabricated from flame cut plates develop residual stresses from each heating process. Flame cutting the edges (simultaneously) induces residual stresses in the flange plate similar to those in Figure 17c, and when the plate is welded into the I-section residual stresses similar to a centre weld are added, as shown in Figure 19b. The resulting residual stress patterns in the flange outstands are shown for each case in Figure 20.

8.4 Inducing Equivalent Stress Profiles in Flange Outstands

Plate specimens were prepared for testing in a plate rig where the plate was to be simply supported on three sides, modelling a flange outstand of a fabricated section. Residual stress profiles were thus required that were equivalent to those in Figure 20. A single edge weld produces yield in tension at the welded edge and less than yield in tension at the unwelded edge, as shown in Figure 17b. This pattern does not resemble the one shown in Figure 20a for cold-cut plates in regard to the stress at the edge opposite the weld, which is also the unsupported edge of the flange outstand. It is important to induce compressive residual stresses at this edge and at the centre of the plate since they affect the buckling behavior. It had been considered to shift the weld closer to the centre so as to reduce the residual stress gradient and obtain a residual stress

pattern in agreement with that shown in Figure 20a. However, the shift required to produce reasonable agreement would exceed a quarter of the plate width, which is deemed unacceptable. It is concluded that it is not possible to induce a residual stress pattern similar to that shown in Figure 20a by placing a weld on a single plate.

The investigation therefore focuses on flame-cut plates, for which the residual stress pattern is similar to that shown in Figure 20b. Two consecutive edge welds were required to produce this pattern, as shown in Figure 18. Since the second weld is laid in a tensile zone, the tendon force is reduced and a stress gradient will arise. Aiming for a constant value of compressive residual stress, more heat is applied in laying the second weld compared to the first. This requires an estimation of the reduction factor (m) in Equation 5, for which the curves given by White (1977b) were used. The target value of compressive residual stress is taken to be 110 MPa, which is a suitable mean of measured values on flanges of I-sections given by Hasham and Rasmussen (1998) and Chick and Rasmussen (1999).

8.5 Welding Process

As the plate specimens were to be used in a plate testing rig, weld deposit along the edges was not desirable. To avoid this an electric-arc welder was used without the addition of weld metal, such that it was operating as a heat source only. The torch was mounted on a motorised, rail-guided trolley that traveled the length of the plates at a constant speed, such that the heat input was constant along the length of the specimen. The magnitude of the heat input per unit length (Q/v) was controlled by the closed circuit voltage (V) and current (I), and the speed (v) of the trolley. The heat input to arc (Q) is given by $Q = V \times I$. The parameters required to induce a compressive stress of 110MPa were determined by substitution into Equations 4 and 5. An estimate of the process efficiency of p=0.45, and reduction factor m=0.7 were used. The test setup is shown in Figure 21.

The residual strains from the welding process were measured with the purpose built extensometer, based on that developed by Denston and White (1977), shown in Figure 22. Small indents were made in the central region of the plates by striking 1mm ball bearings with a hammer. The extensometer was seated in the indentations before and after the welds were laid, and the distance between the two holes was measured. From these readings the weld shrinkage strain may be deduced, and the stress is calculated by multiplying the strain by the material Young's modulus. Readings were taken on each surface of the plate and averaged to obtain the membrane stresses. An example of the indentation layout is given in Figure 23.

8.6 Results of Welding Process

Forty plate specimens were welded along both longitudinal edges consecutively. Table 4 shows a sample of the results for the plates of width 120mm. It is noted that the required current was set on the welder, and the machine ran at a voltage that was affected by the distance of the arc from the plate. The measured closed circuit voltage was generally in the range of 9-12 Volts, varying slightly along the length of the plate. The voltage values in Table 4 are average values for the weld runs.

The centreline of the weld from the edge was 5mm for plate widths less than 100mm, and 10mm for those exceeding 100mm. The average process efficiency of the former was found to be 0.416, and the latter 0.507. This is a result of increased heat loss when the weld is placed closer to the edge of the plate. The process efficiency is calculated from Equations 4 and 5, where the reduction factor (m) is deduced from the measured stress gradient and the tendon force (F) from the measured stress magnitude. Figure 24 shows the process efficiency to increase slightly with plate width. All the plates were positioned on heat resistant bricks then clamped with steel clamps to minimise bending near the line of the weld (Figure 21). As the

plate width increased, comparatively less of the specimen was seated on the bricks, and therefore less heat was lost through the bricks and clamps. The process efficiency therefore increases. The process efficiency is largely dependant on the experimental setup.

As the process efficiency increases, so does the tendon force in Equation 4 for the first weld, and consequently the value of tensile stress produced at the other edge by the first weld increases also. The second weld is thus being laid in a more highly stressed material than was expected from the assumption that the process efficiency would remain constant, and consequently as the plate width increases the calculated reduction factor (*m*) decreases (Figure 25). The average value of *m* was found to be 0.701, which is very close to the assumed constant value of 0.7. Where the assumed value of *m* is different from the actual value, a gradient exists in the residual stress profile. The average difference in stress between the two edges of the compressive regions for all specimens is 15%. The average compressive stress is 104MPa, with a standard deviation of 16MPa. Results for the residual stresses induced in all specimens, and gradients of stress in the compression region are presented in Table 5. The gradient is defined as the change in stress between measurement points 1 and 5 (see Figure 23), divided by the distance between these points.

9 REDUCTION OF FORCE AND MOMENT MEASUREMENTS

9.1 Total Force

The total axial load applied to the specimen is taken as the axial load applied by the primary compression actuator, in addition to the axial load applied by the secondary bending actuator. The load value on the secondary actuator may be positive or negative, depending on the load case.

For the case of pure compression, after the unsupported edge buckles the net resistance becomes eccentric and the loading platens try to rotate. The secondary actuator essentially applies load in order to resist this rotation, in the opposite direction to the load applied by the primary actuator (Figure 26a). Therefore the total load applied to the specimen is the load applied by the primary rig, less the load applied by the secondary rig. The load case of compressive strain applied at the supported edge and zero strain at the unsupported edge involves loads applied by the secondary actuator in the opposite direction also (Figure 26a), therefore the total load is calculated the same way as that for the pure compression case. The load case of compressive strain applied at the unsupported edge and zero strain applied at the supported edge involves loads applied by the secondary actuator in the same direction as the primary actuator (Figure 26b). The total load for this case is calculated as the load applied by the primary actuator in addition to that applied by the secondary actuator.

For the three previous load cases the total applied load is compressive. For the case of pure bending with compression at the unsupported edge however, the redistribution of forces after buckling causes the net force to be tensile (Figure 26c). The total tensile force is then the force applied by the primary actuator, less that applied by the secondary actuator.

9.2 Total Moment

There are two contributions to the total moment. The first is the moment due to the load applied by the secondary actuator, and is calculated as the load applied multiplied by the moment lever arm, being the perpendicular distance between the centreline of the secondary actuator and the centreline of the point of rotation (Figure 27b).

Since the point of rotation is at a certain distance behind the loaded edge of the specimen, as the lever arms rotate the specimen is transformed as a rigid body in the transverse direction. The centreline of the specimen is then no longer parallel to the line joining the points of rotation. The load applied by the primary actuator is applied through the pin joints, at the points of rotation, therefore as the lever arms rotate the load applied by the primary actuator is eccentric to the centreline of the specimen. This creates an additional moment, which may act in addition to or against the moment applied by the secondary actuator, depending on the load case. At every reading, this moment is calculated as the current value of load applied by the primary actuator multiplied by the current value of eccentricity. The eccentricity is calculated using Equations 6-9, with reference to Figure 27a, where:

D = the distance between the point of rotation and the centreline of the lever arms
R = the distance between the point of rotation and the loaded edge of the specimen
s = the stroke of the secondary actuator

For the pure bending case (Figure 26c), the moment due to the eccentricity is subtracted from the moment from the secondary actuator. For the case of compressive strain at the unsupported edge and zero strain at the supported edge (Figure 26b), and the case of compressive strain at the supported edge and zero strain at the unsupported edge (Figure 26a), the moment due to the eccentricity is added.

$$sin(\phi) = \frac{D + s}{\sqrt{\left(D^2 + Moment\_Lever\_Arm^2\right)}} \tag{6}$$

$$tan(\beta) = \frac{D}{Moment\_Lever\_Arm} \tag{7}$$

$$\alpha = \phi - \beta = sin^{-1}\left(\frac{D + s}{\sqrt{\left(D^2 + Moment\_Lever\_Arm^2\right)}}\right) - tan^{-1}\left(\frac{D}{Moment\_Lever\_Arm}\right) \tag{8}$$

$$Eccentricity = R \times \sin(\alpha) \tag{9}$$

An independent measurement system to measure the transverse displacement of the specimens was not present in the tests, however a small number of readings were taken for specimen c21801. For this specimen the centreline shift at the final point in the test was measured as approximately 90mm. The eccentricity calculation for this specimen produces a value of 95.9mm at the final point in the test.

10 ELASTIC CRITICAL BUCKLING STRESS RESULTS

10.1 Experimental Elastic Buckling Stress

The elastic critical buckling stress is estimated using the Load vs Lateral Displacement Squared method, as described by Venkataramaiah and Roorda (1982), whereby a tangent to the curve is drawn in the post-buckling range, and the intersection point of this line with the vertical (load) axis gives the elastic buckling load, for the case of pure compression. For the case of pure bending, the vertical axis is the applied moment, and the buckling moment is determined in the same way. The buckling stress is determined from the applied load or moment from engineering theory, as described in Section 12.2. For the load cases with compressive stress at one longitudinal edge and zero stress at the other edge, the vertical axis is the total stress. The total stress is the sum of the stresses applied by the primary and secondary actuators, based on engineering theory as described in Section 12.2, and is the stress at the most heavily loaded longitudinal edge. It is noted that a certain amount of discretion is required when drawing the tangent, and the result for the buckling stress can vary quite considerably depending on how the tangent is drawn. The method is approximate then, however a

reasonable estimation of the buckling stress may be achieved. Curves of Load vs Lateral Displacement Squared are shown in Appendix C for all specimens, and specimens that undergo elastic buckling have the tangent drawn on the curves. The experimental buckling stresses are presented in Table 6 for specimens that undergo elastic buckling, being those specimens with a nominal slenderness of 1.55 and 2.17.

10.2 Theoretical Elastic Buckling Stress

The theoretical elastic critical buckling stresses are calculated using Equation 2 and are given in Table 6, using nominal plate widths and thicknesses. The buckling coefficient (k) for each load case is given in Table 1. These are the buckling coefficients calculated from THINWALL for rectangular plates simply supported on three sides, for infinitely long plates. The buckling coefficient for the load case c2 was taken as $k = 1.24$, which is the solution from Bulson (1970) for an unstiffened plate with fixed loaded edges in pure bending (with compression at the unsupported edge). The theoretical buckling stresses for this load case (shaded in Table 6) were calculated using Equation 2.

10.3 Comparison of Experimental and Theoretical Elastic Buckling Stresses

Comparisons of the experimental and theoretical elastic critical buckling stresses in Table 6 for unwelded specimens show good agreement for the most slender specimens. The average difference between experimental and theoretical elastic buckling stresses is 4%, with a standard deviation of 10%, for specimens with simply supported loaded edges.

10.4 Buckled Shapes

The buckled shapes of all specimens may be viewed in the plots of the Lateral Displacement Profiles in Appendix B. In general, the results show that unstiffened plates will buckle in a single half-wavelength under all stress gradients, with the maximum lateral deflection occurring approximately at the mid-length of the plate. In the transverse direction, if a section is taken at any point along the length of the plate, the buckled shape is such that a straight line is formed from the supported edge to the unsupported edge. As the load increases past the point of buckling, the same buckled shape is magnified. As the ultimate load is approached however, localisation occurs, and the maximum deflection localises to one end of the plate. In this region plastification then occurs, and the remainder of the plate elastically unloads, and the plate straightens out away from the localised failure. In the post-ultimate range, lateral deflections continue to increase in the localised plastic zone, and correspondingly so does the rotation of the end bearings at the end where localisation has occurred. For the load case of compressive strain at the supported edge and zero at the unsupported edge, the localisation occurs noticeably closer to the supported edge than for the other load cases.

The magnitude of the lateral displacement at the elastic buckling stress for the most slender specimen under pure compression is of the order of the plate thickness. At ultimate the lateral displacement is of the order of four times the plate thickness. It is shown in the plots that the magnitude of lateral deflections increases with slenderness, as one would expect. Similarly, when compared with the case of pure compression, the load case of compressive strain at the unsupported edge and zero at the supported edge produces larger lateral deflections, and the load case of compressive strain at the supported edge and zero at the unsupported edge produces smaller lateral deflections. The load case of pure bending with compression at the unsupported edge produces the largest magnitudes of lateral displacements.

Specimens that do not undergo elastic buckling generally remain straight until approximately the ultimate condition, and lateral displacements form in a localised shape, displaying little or none of the single half-wave buckled shape of slender specimens.

10.5 Effects of Geometric Imperfections on Buckling

A perfectly flat unstiffened plate will not displace laterally until the elastic buckling stress is reached, at which time lateral displacements will occur in a classic single half-wave shape, with the maximum deflection at the mid-length of the plate. An initially imperfect plate, however, will displace laterally well before the buckling stress, as is shown in the Lateral Displacement Profiles in Appendix B. In general, the geometric imperfections were in a single half-wave, however often the maximum imperfection was not exactly at the mid-length of the specimen. It was noted that often the lateral displacements localised at the same end as the maximum imperfection, however the buckled shape did not appear to be greatly affected by the imperfections, except that in general the specimen buckled on the same side vertically (i.e. either up or down) as the imperfection.

10.6 Effects of Residual Stresses on Buckling

The presence of residual stresses due to welding did not appear to have affected the buckled shape, except for the widest specimens of nominal width 255mm and 355mm. The width of these plates was such that high heat input was required in the welding process in order to induce the required magnitude of residual stresses. These specimens contained pronounced lateral displacements due to the welding process, often in several half-wavelengths, as a result of elastic buckling of the plate. While the lateral displacements were contained by the insertion of the specimen into the plate testing rig, the displacement profiles under loading show up to four half-wavelengths for the buckled shapes (Figures B26, B27, B30, and B31).

In general, the presence of welding residual stresses increased the experimental elastic buckling stress (Table 6). The buckling stress for slender welded specimens is on average 23% higher than those for unwelded specimens. The is due to the residual stress pattern, where tension yield blocks existed at both longitudinal edges in order to model flame cut plates. The presence of a tension yield block at the unsupported edge had a stablising effect, increasing the buckling stress by restraining to some extent the formation of lateral displacements of the edge. It is noted that examination of the ultimate strengths of the plates in the companion report Bambach and Rasmussen (2002b), shows that the average ultimate strength of welded plates is only marginally less than those for unwelded plates.

11 VERIFICATION OF THE RIG

11.1 Elastic Buckling Stresses

Comparisons of experimental and theoretical buckling stresses (Table 6) show sufficient agreement such that one can assume the experimental setup is congruent with the theoretical model. Since the theoretical model assumes that the plates have pure simple support on three sides, we can assume that the simple supports of the plate testing rig are providing negligible rotational restraint to the three edges.

11.2 Post-Buckling Strength

As mentioned in the introduction, if plates simply supported on three sides are tested in rigs that apply load at constant eccentricity, little post-buckling strength is achieved. An important part of the verification of the

rig developed by the authors then, is that post-buckling strength is being achieved, such that the ultimate condition is reached. The curves of total stress vs lateral displacement squared in Appendix C, particularly for the most slender specimens of each load case, show that stresses far in excess of the buckling stress are being achieved.

12 ULTIMATE STRENGTH RESULTS

12.1 Force and Moment vs Axial Displacement Results

The plate test results are presented for all tests as curves of force (F) and moment (M) against axial displacement of the displaced longitudinal edge in Appendix D. The axial displacement is that calculated from the strain gauges and LVDTs by the method described in Section 4. The force and moment values are the reduced values from the primary and secondary actuators as described in Section 9. Figures D1-D5 show test results for the case of pure compression, Figures D6-D10 show test results of the load case of compressive strain at the unsupported edge and zero strain at the supported edge, Figures D11-D15 show test results of the load case of compressive strain at the supported edge and zero strain at the unsupported edge, and Figures D16-D25 show test results and Abaqus results (described in a companion report Bambach and Rasmussen 2002b) of the load case of pure bending with compressive strain at the unsupported edge.

12.2 Stress from the Force and Moment vs Axial Displacement Results

The stress from the applied force (f_c) and the stress from the applied moment (f_m) are calculated as the stresses on the gross area from Equations 10 and 11 respectively. The sum of the stresses at the most heavily strained edge gives the maximum stress on the plate specimen. The stresses from the applied force and moment are plotted with the maximum (total) stress against axial displacement in Appendix E, for the load cases of compressive strain at the unsupported edge and zero strain at the supported edge (Figures E1-E20), and compressive strain at the supported edge and zero strain at the unsupported edge (Figures E21-E40).

$$f_c = \frac{F}{bt} \tag{10}$$

$$f_m = \frac{My}{I} = \frac{6M}{b^2 t} \tag{11}$$

12.3 Total Stress vs Axial Displacement Results

In order to compare the total stress vs axial displacement curves for various slenderness ratios, an unwelded specimen of each of the five nominal slenderness ratios tested is plotted, for each of the four tested load cases. These curves are presented in Figures 28-31.

12.4 Ultimate Condition

The curves of stress vs axial displacement are used to determine the ultimate condition. Examples of these curves are given in Figures 32-35. For the case of pure compression, the ultimate condition is taken as the point at which the compressive stress is a maximum (Figure 28). This point corresponds to an ultimate strain of approximately the yield strain for all slenderness ratios. For the case of pure bending with compressive strain at the unsupported edge, the ultimate condition is taken as the point at which the bending stress is a maximum (Figure 33). Due to limitations of the strokes of the actuators, the ultimate condition could not be reached in the tests. Analysis using the FEM program Abaqus is compared with the test results for the range tested, and used to determine the ultimate moment (Figure 33). The Abaqus model incorporates the

measured material properties and geometric imperfections. For the case of compressive strain at the supported edge and zero strain at the unsupported edge, the compressive stress and the bending stress peak at approximately the same value of axial shortening and reduce thereafter, such that the total stress peaks at the same value of axial shortening, and this point is taken as the ultimate condition (Figure 34). The strain at ultimate is printed on the curves in Figures 33,34,35.

For the case of compressive strain at the unsupported edge and zero strain at the supported edge, the compressive stress and the bending stress peak at approximately the same value of axial shortening and reduce thereafter, for the less slender specimens only. As the slenderness increases, the specimens tend to maintain compressive stress while the bending stress decreases. For the most slender specimens, the stress due to the compressive force continues increasing while the bending stress decreases, causing the total stress to approximately maintain its maximum value up to large values of axial shortening (Figure 35). For this load case the ultimate total stress is taken as that corresponding to an axial strain of two times the yield strain. This value of axial strain was chosen due to considerations of the ultimate strain in sections that contain unstiffened elements under similar strain gradients, being I-sections and channel sections in minor axis bending, as discussed in the companion paper Bambach and Rasmussen (2002a).

12.5 Ultimate Force and Moment Results

The ultimate force and moment values from the plate tests for uniform compression and strain gradient are presented in Tables 7-9. The tables give ultimate force and moment values (about the centre-width of the specimen), magnitudes of compressive residual stresses, plate dimensions and the ratio of the ultimate strain to the yield strain. The force and moment values from the plate tests for uniform bending (with compression at the unsupported edge), when the maximum strain on the plate is the yield strain, are presented in Table 10. The ultimate force and moment values from the Abaqus analyses for uniform bending (with compression at the unsupported edge) are presented in Table 11.

13 CONCLUSIONS

A dual-actuator plate test rig developed for testing unstiffened elements under strain gradients is presented. Plate test results of 80 specimens under a variety of strain gradients and slenderness ratios are presented. The plate specimens include both unwelded and welded specimens. The plate test results are used to establish effective width equations for unstiffened elements under stress gradients in a companion report (Bambach and Rasmussen 2002b), where both elastic and plastic effective widths are derived. In an additional report (Bambach and Rasmussen 2002a), the effective width equations are used in conjunction with inelastic considerations of the effective section, to produce a general design procedure for sections in bending that contain unstiffened elements under stress gradients.

14 REFERENCES

AS 1391 (1991). *Australian Standard. Methods for Tensile Testing of Metals*. Standards Australia, Sydney.

Bambach, M. R. and Rasmussen, K. J. R. (2002a). "Design models for Thin-Walled Sections in Bending containing Unstiffened Elements." *Research Report R820*, Department of Civil Engineering, University of Sydney, Sydney.

Bambach, M. R. and Rasmussen, K. J. R. (2002b). "Elastic and Plastic Effective Width Equations for Unstiffened Elements." *Research Report R819*, Department of Civil Engineering, University of Sydney, Sydney.

Beale, R. G., Godley, M. H. R. and Enjily, V. (2001). "A Theoretical and Experimental Investigation into Cold-formed channel sections in Bending with the Unstiffened Flanges in Compression." *Computers and Structures*, 79, pp. 2403-2411.

Bradfield, C. D. (1979). "Tests on Single Plates under In-Plane Compression with Controlled Residual Stresses and Out-of-Flatness." *Report CUED/C-Struct/TR.78*, University of Cambridge, UK.

Bulson, P. S. (1970). *The Stability of Flat Plates*. Chatto and Windus, London.

Chick, C. G. and Rasmussen, K. J. R. (1999). "Thin-Walled Beam-Columns. 2:Proportional Loading Tests." *Journal of the Structural Division, ASCE*, 125(11), pp. 1267-1276.

Denston, R. J. and White, J. D. (1977). "An Electric Demountable Extensometer." *Report CUED/C-Struct/TR.61*, University of Cambridge, UK.

Dwight, J. B. and Moxham, K. E. (1971). "Further tests on Welded Box Columns." *Report CUED/C-Struct/TR.15*, University of Cambridge, UK.

Hasham, A. S. and Rasmussen, K. J. R. (1998). "Section Capacity of Thin-Walled I-section Beam-columns." *Journal of Structural Engineering, ASCE*, 124(4), pp. 351-359.

Kamtekar, A. G. (1974). "An Experimental Study of Welding Residual Stresses." *Report CUED/C-Struct/TR.39*, University of Cambridge, UK.

Moxham, K. E. (1971). "Buckling Tests on Individual Welded Steel Plates in Compression." *Report CUED/C-Struct/TR.3*, University of Cambridge,

Papangelis, J. P. and Hancock, G. J. (1995). "Computer Analysis of Thin-Walled Structural Members." *Computers and Structures*, 56(1), pp. 157-176.

Rasmussen, K. J. R. (1994). "Design of Thin-Walled Columns with Unstiffened Flanges." *Engineering Structures*, 16(5), pp. 307-316.

Rhodes, J., Harvey, J. M. and Fok, W. C. (1975). "The Load-Carrying Capacity of Initially Imperfect Eccentrically Loaded Plates." *International Journal of Mechanical Sciences*, 17, pp. 161-175.

Rusch, A. and Lindner, J. (2001). "Remarks to the Direct Strength Method." *Thin-Walled Structures*, 39, pp. 807-820.

Venkataramaiah, K. R. and Roorda, J. (1982). "Analysis of Local Plate Buckling Data". *Proc., Sixth International Specialty Conference on Cold-Formed Steel Structures*, pp.

White, J. D. (1977a). "Longitudinal Shrinkage of a Single Pass Weld." *Report CUED/C-Struct/TR.57*, University of Cambridge, UK.

White, J. D. (1977b). "Longitudinal Stresses in a Member Containing Non-Interacting Welds." *Report CUED/C-Struct/TR.58*, University of Cambridge, UK.

White, J. D. (1977c). "Longitudinal Stresses in Welded T-Sections." *Report CUED/C-Struct/TR.60*, University of Cambridge, UK.

15 TABLES

Nominal Slenderness	Nominal Plate Width (mm)				
	Load Case c0 k=0.425	Load Case c1 k=0.590	Load Case c2 k=0.885	Load Case c3 k=1.77	Load Case c-2 k=24.2
0.75	60	70	85	120	455
1	80	95	115	165	605
1.25	100	120	145	205	755
1.55	125	145	180	255	935
2.17	175	205	250	355	1310

Nominal plate thickness is 5mm
Nominal plate length is 5 x Plate width

Load case c0

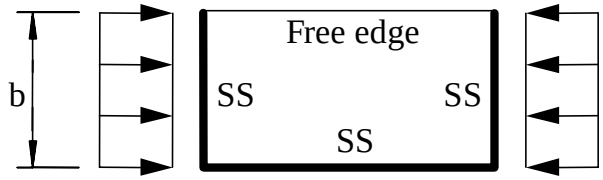

Load case c1

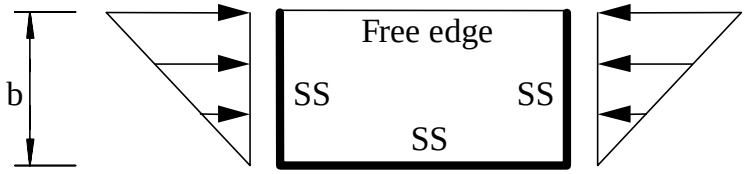

Load case c2

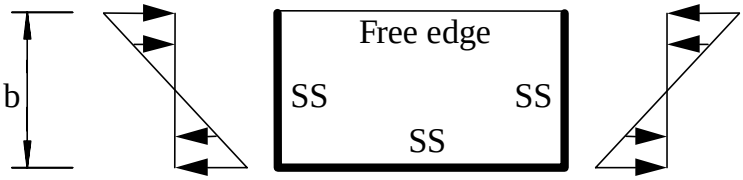

Load case c3

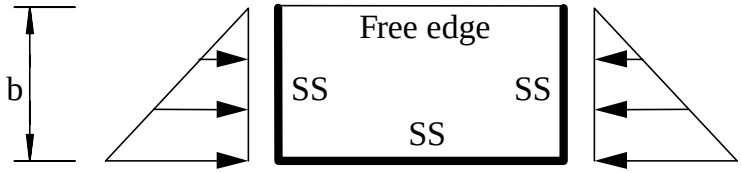

Load case c-2
Abaqus simulation only

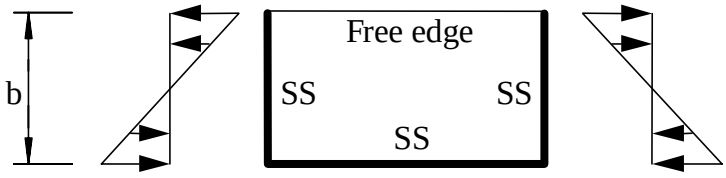

Table 1 : Nominal plate widths for all load cases

	Nominal	Measured			
Plate	$\sigma_{0.2}$ (MPa)	E (GPa)	$\sigma_{0.2}$ (MPa)	σ_u (MPa)	ε_u (%)
1	300	202	271	479	18
2	300	199	317	504	20

Table 2: Nominal and measured material properties

Specimen		Average* Maximum Imperfection of the Unsupported Edge (mm)
c0	60	0.367
c0	80	0.311
c0	100	0.328
c0	125	0.483
c0	175	1.006
c1	70	0.368
c1	95	0.160
c1	120	0.749
c1	145	0.426
c1	205	1.156
c3	120	0.664
c3	165	0.712
c3	205	1.118
c3	255	2.010
c3	355	1.935
c2	85	0.319
c2	115	0.723
c2	145	0.960
c2	180	1.215
c2	250	2.515
Mean:		0.876

* Average of four plates

Table 3 : Summary of Geometric Imperfection Results

			Experiment Parameters				Results			
	Nominal Width (mm)	Nominal Thickness (mm)	Voltage (V)	Current (Amps)	Speed (mm/sec)	Q/v (kJ/m)	m	p	Pt 1 (MPa)	Pt 5 (MPa)
Weld1	120	5	10	105	5.04	208.25				
Weld2	120	5	11	148	5.17	314.75	0.717	0.530	-120	-129
Weld1	120	5	10	105	5.17	203.00				
Weld2	120	5	11	148	5.13	317.46	0.694	0.499	-111	-117
Weld1	120	5	10	105	5.45	192.50				
Weld2	120	5	10	148	5.17	286.13	0.729	0.478	-107	-111

Table 4: Sample of Welding Results for Plate Width 120mm

Specimen	Stress at position 1 (MPa)	Stress at position 2 (MPa)	Stress at position 3 (MPa)	Stress at position 4 (MPa)	Stress at position 5 (MPa)	Average (MPa)	Gradients	Change in Stress (MPa)
c0 60 w1	72	80	72	75	76	75	0.07	1
c0 60 w2	84	93	92	86	95	90	0.21	4
c1 70 w1	129	101	123	104	95	110	-0.61	18
c1 70 w2	63	70	84	90	99	81	0.87	26
c0 80 w1	0	79	77	96	105	89	0.62	25
c0 80 w2	109	100	96	83	74	92	-0.63	25
c2 85 w1	101	94	103	94	100	98	-0.03	1
c2 85 w2	109	105	106	96	101	103	-0.18	7
c1 95 w1	117	105	125	130	136	122	0.46	18
c1 95 w2	79	100	104	127	126	107	0.86	35
c0 100 w1	83	85	86	86	84	85	0.02	1
c0 100 w2	66	67	87	67	98	77	0.45	18
c2 115 w1	63	74	89	104	88	83	0.56	22
c2 115 w2	74	77	87	97	105	88	0.58	23
c1 120 w1	120	131	97	138	129	123	0.13	7
c1 120 w2	111	102	115	119	117	113	0.17	8
c3 120 w1	98	109	131	137	155	126	0.81	41
c3 120 w2	85	111	107	119	90	102	0.11	5
c0 125 w1	92	95	104	101	103	99	0.15	8
c0 125 w2	83	104	102	115	119	104	0.47	24
c1 145 w1	92	93	110	115	141	110	0.57	34
c1 145 w2	97	110	113	110	111	108	0.14	8
c2 145 w1	118	121	99	110	100	109	-0.23	14
c2 145 w2	97	102	107	122	130	112	0.41	25
c3 165 w1	94	91	88	85	95	90	-0.01	1
c3 165 w2	93	85	84	91	94	89	0.03	2
c0 175 w1	128	118	118	102	114	116	-0.16	13
c0 175 w2	114	109	119	109	121	114	0.05	4
c2 180 w1	140	126	131	134	130	132	-0.05	4
c2 180 w2	141	118	131	111	116	123	-0.21	16
c1 205 w1	146	123	111	118	103	120	-0.33	26
c1 205 w2	130	125	113	124	107	120	-0.17	13
c3 205 w1	147	141	106	106	105	121	-0.42	34
c3 205 w2	148	121	136	109	111	125	-0.31	25
c2 250 w1	125	136	86	111	104	112	-0.16	19
c2 250 w2	135	108	99	105	99	109	-0.17	21
c3 255 w1	93	121	112	109	82	103	-0.08	10
c3 255 w2	122	117	113	115	107	115	-0.08	9
c3 355 w1	117	67	45	73	87	78	-0.08	15
c3 355 w2	116	93	57	55	114	87	-0.07	12
* average of absolute values					Average:	104	[0.29]*	16
					Standard Deviation:	16	0.25	11

Table 5: Results of stresses induced by welding (positive denotes compression)

Unwelded Specimens					**Welded Speicmens**			
Specimen	Elastic Buckling Stress **Test** (MPa)	Average Elastic Buckling Stress **Test** (MPa)	Nominal Elastic Buckling Stress **Theory*** (MPa)	Difference between **Test** and **Theory**	Specimen	Elastic Buckling Stress **Test** (MPa)	Average Elastic Buckling Stress **Test** (MPa)	Difference between Welded and Unwelded
c0 100 1	228				c0 100 w1	180		
c0 100 2	172	200	192	4.2%	c0 100 w2	162	171	-14.5%
c0 125 1	117				c0 125 w1	125		
c0 125 2	147	132	122	8.2%	c0 125 w2	141	133	0.6%
c0 175 1	63				c0 175 w1	97		
c0 175 2	78	70	63	11.6%	c0 175 w2	91	94	34.1%
c1 120 1	170				c1 120 w1	208		
c1 120 2	192	181	185	-2.2%	c1 120 w2	192	200	10.5%
c1 145 1	158				c1 145 w1	180		
c1 145 2	133	146	127	14.6%	c1 145 w2	189	185	26.8%
c1 205 1	68				c1 205 w1	85		
c1 205 2	74	71	63	12.7%	c1 205 w2	103	94	32.4%
c3 205 1	175				c3 205 w1	265		
c3 205 2	168	172	190	-9.7%	c3 205 w2	355	310	80.8%
c3 255 1	83				c3 255 w1	175		
c3 255 2	130	107	123	-13.4%	c3 255 w2	140	158	47.9%
c3 355 1	96				c3 355 w1	75		
c3 355 2	43	70	63	10.3%	c3 355 w2	75	75	7.9%
c2 145 1	211				c2 145 w1	234		
c2 145 2	197	204	268	-23.9%	c2 145 w2	214	224	9.8%
c2 180 1	178				c2 180 w1	252		
c2 180 2	193	185	173	7.0%	c2 180 w2	289	270	46.0%
c2 250 1	157				c2 250 w1	157		
c2 250 2	157	157	90	74.9%	c2 250 w2	131	144	-8.5%
			Average:	4.02%			Average:	22.81%
			Standard Deviation:	10.20%			Standard Deviation:	27.26%

* Using THINWALL

Table 6: Results of elastic buckling stresses for slender specimens with nominal slenderness ratios of 1.55 and 2.17

Specimen			*b* (mm)	*t* (mm)	Yield Stress (MPa)	Residual stress (MPa)	Ultimate Force (kN)	Ultimate strain/ yield strain
c0	60	1	61.2	4.77	272.2	0	78.8	1.3
c0	60	2	60.6	4.77	272.2	0	82.4	1.2
c0	60	w1	61.0	4.77	272.2	75	80.2	1.5
c0	60	w2	60.5	4.77	272.2	90	73.2	1.2
c0	80	1	80.0	4.75	317.2	0	95.1	1.0
c0	80	2	79.9	4.75	317.2	0	103.0	0.9
c0	80	w1	79.9	4.75	317.2	89	97.3	1.0
c0	80	w2	79.7	4.75	317.2	92	103.5	1.0
c0	100	1	100.4	4.77	272.2	0	114.2	0.8
c0	100	2	100.3	4.77	272.2	0	94.3	0.9
c0	100	w1	100.4	4.77	272.2	85	97.5	0.8
c0	100	w2	100.3	4.77	272.2	77	88.5	1.0
c0	125	1	125.6	4.77	272.2	0	94.8	0.8
c0	125	2	125.8	4.77	272.2	0	94.3	0.6
c0	125	w1	125.5	4.77	272.2	99	85.5	0.9
c0	125	w2	125.3	4.77	272.2	104	100.7	0.8
c0	175	1	175.2	4.77	272.2	0	123.3	1.1
c0	175	2	175.0	4.77	272.2	0	127.0	0.9
c0	175	w1	175.4	4.77	272.2	116	113.4	1.2
c0	175	w2	175.2	4.77	272.2	114	111.3	1.1
							Mean:	1.0

Table 7: Test results – Pure compression

Specimen			*b* (mm)	*t* (mm)	Yield stress (MPa)	Residual stress (MPa)	Ultimate force (kN)	Ultimate moment about centre (kNm)	Ultimate strain/ yield strain
c1	70	1	69.7	4.75	317.2	0	57.3	2.66	2
c1	70	2	70.2	4.75	317.2	0	65.7	3.10	2
c1	70	w1	69.8	4.75	317.2	110	50.4	2.65	2
c1	70	w2	69.6	4.75	317.2	81	49.9	2.65	2
c1	95	1	95.3	4.77	272.2	0	58.2	4.01	2
c1	95	2	95.3	4.77	272.2	0	60.9	3.99	2
c1	95	w1	95.2	4.77	272.2	122	54.9	3.70	2
c1	95	w2	95.4	4.77	272.2	107	53.2	3.72	2
c1	120	1	119.9	4.77	272.2	0	61.8	4.10	2
c1	120	2	119.9	4.77	272.2	0	68.0	4.99	2
c1	120	w1	119.9	4.77	272.2	123	62.3	4.18	2
c1	120	w2	119.8	4.77	272.2	113	64.0	4.40	2
c1	145	1	145.3	4.77	272.2	0	57.5	4.77	2
c1	145	2	145.0	4.77	272.2	0	63.0	5.28	2
c1	145	w1	144.7	4.77	272.2	110	46.2	3.76	2
c1	145	w2	144.4	4.77	272.2	108	53.7	4.16	2
c1	205	1	204.7	4.75	317.2	0	58.3	6.90	2
c1	205	2	204.6	4.75	317.2	0	60.3	6.89	2
c1	205	w1	204.3	4.75	317.2	120	54.3	6.41	2
c1	205	w2	204.7	4.75	317.2	120	53.5	7.40	2
								Mean:	2

Table 8: Test results – Compressive strain at the unsupported edge, zero at the supported edge

Specimen			*b* (mm)	*t* (mm)	Yield stress (MPa)	Residual stress (MPa)	Ultimate force (kN)	Ultimate moment about centre (kNm)	Ultimate strain/ yield strain
c3	120	1	119.9	4.77	272.2	0	111.9	8.73	1.7
c3	120	2	120.0	4.77	272.2	0	100.3	8.23	1.7
c3	120	w1	120.0	4.77	272.2	126	102.2	8.41	1.3
c3	120	w2	119.8	4.77	272.2	102	107.2	8.98	2.2
c3	165	1	165.2	4.77	272.2	0	137.2	16.13	1.6
c3	165	2	164.7	4.77	272.2	0	117.6	13.77	1.5
c3	165	w1	165.3	4.77	272.2	90	123.9	15.60	2.3
c3	165	w2	165.1	4.77	272.2	89	137.1	16.54	2.1
c3	205	1	204.5	4.75	317.2	0	157.3	25.07	1.7
c3	205	2	204.6	4.75	317.2	0	171.1	26.45	1.8
c3	205	w1	204.9	4.75	317.2	121	165.2	25.78	2.0
c3	205	w2	204.6	4.75	317.2	125	172.4	27.48	2.3
c3	255	1	254.2	4.75	317.2	0	168.8	33.74	1.2
c3	255	2	254.2	4.75	317.2	0	172.8	34.56	1.4
c3	255	w1	254.7	4.75	317.2	103	159.0	32.88	1.9
c3	255	w2	254.5	4.75	317.2	115	158.3	33.17	2.0
c3	355	1	354.6	4.75	317.2	0	166.4	49.71	1.1
c3	355	2	354.6	4.75	317.2	0	167.9	49.94	1.1
c3	355	w1	354.6	4.75	317.2	78	154.4	47.31	1.7
c3	355	w2	354.5	4.75	317.2	87	155.9	51.33	2.1
								Mean:	1.7

Table 9: Test results – Compressive strain at the supported edge, zero at the unsupported edge

Specimen			*b* (mm)	*t* (mm)	Yield stress (MPa)	Residual stress (MPa)	Tensile force (kN)	Yield moment about centre (kNm)	Strain/ yield strain
c2	85	1	85.1	4.77	272.2	0	0	1.97	1.0
c2	85	2	85.3	4.77	272.2	0	0	2.03	1.0
c2	85	w1	85.0	4.77	272.2	98	0	1.77	1.0
c2	85	w2	84.9	4.77	272.2	103	0	1.97	1.0
c2	115	1	115.7	4.77	272.2	0	N/A	N/A	N/A
c2	115	2	114.8	4.77	272.2	0	0	2.95	1.0
c2	115	w1	115.2	4.77	272.2	83	0	2.79	1.0
c2	115	w2	115.4	4.77	272.2	88	0	2.73	1.0
c2	145	1	145.0	4.77	272.2	0	3.00	4.19	1.0
c2	145	2	145.0	4.77	272.2	0	11.50	3.73	1.0
c2	145	w1	145.0	4.77	272.2	109	0	3.88	1.0
c2	145	w2	144.6	4.77	272.2	112	0	3.79	1.0
c2	180	1	180.1	4.75	317.2	0	0	5.60	1.0
c2	180	2	179.1	4.75	317.2	0	30.82	6.38	1.0
c2	180	w1	179.7	4.75	317.2	132	0.00	6.03	1.0
c2	180	w2	179.7	4.75	317.2	123	36.26	6.35	1.0
c2	250	1	249.9	4.75	317.2	0	59.28	8.53	1.0
c2	250	2	244.0	4.75	317.2	0	46.57	9.21	1.0
c2	250	w1	249.7	4.75	317.2	112	22.08	8.28	1.0
c2	250	w2	249.7	4.75	317.2	109	17.98	7.23	1.0

Table 10: Tests results – Pure bending

Specimen		*b* (mm)	*t* (mm)	Yield stress (MPa)	Residual stress (MPa)	Ultimate force (kN)	Ultimate moment about centre (kNm)	Ultimate strain/ yield strain
c2	85	85	5	272.2	0	62.1	3.47	45
c2	115	115	5	272.2	0	85.7	5.73	38
c2	145	145	5	272.2	0	108.8	8.78	39
c2	180	180	5	317.2	0	150.3	13.74	29
c2	250	250	5	317.2	0	212.5	26.97	28

Table 11: Abaqus (FEM) results – Pure bending

16 FIGURES

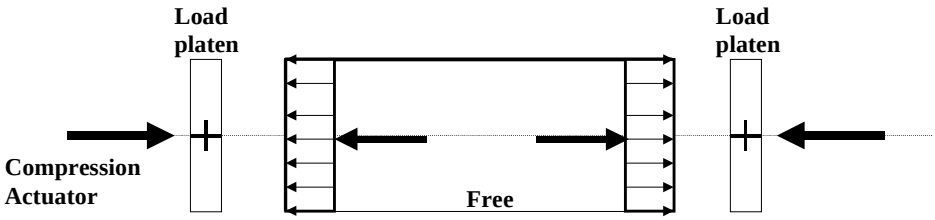

(a) Pre-Buckled Stress Distribution

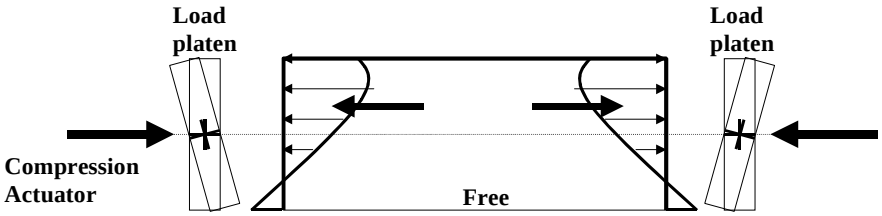

(b) Post-Buckled Stress Distribution

Figure 1 : Unstiffened plate tests under constant load eccentricity

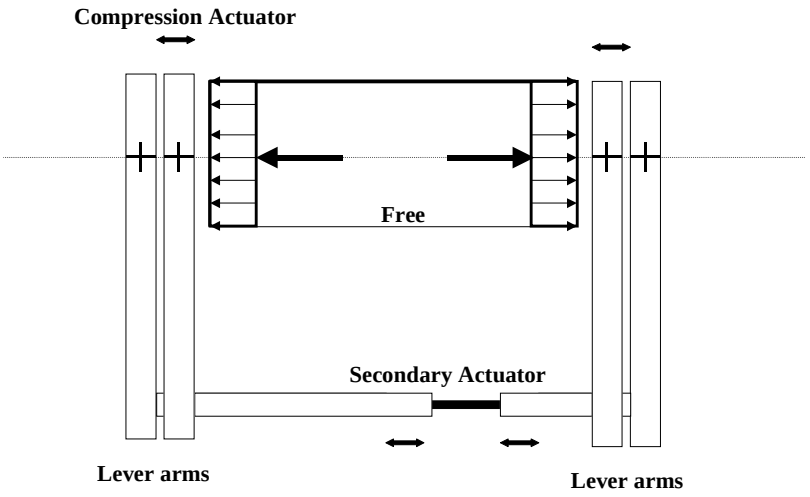

(a) Pre-Buckled Stress Distribution

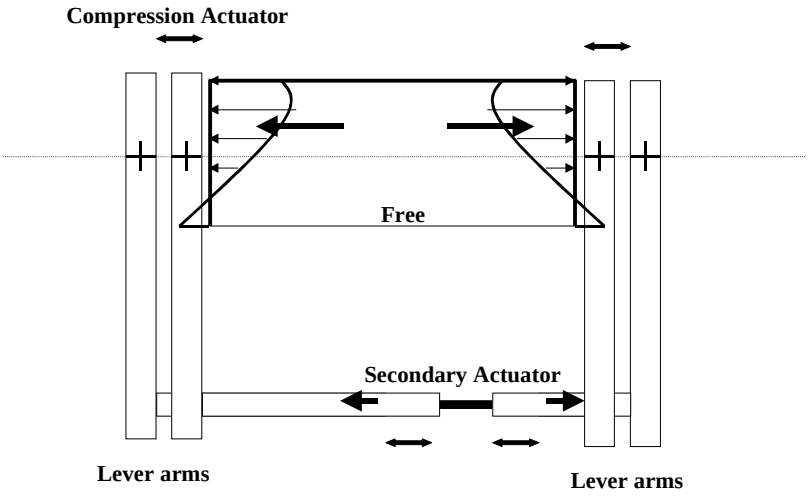

(b) Post-Buckled Stress Distribution

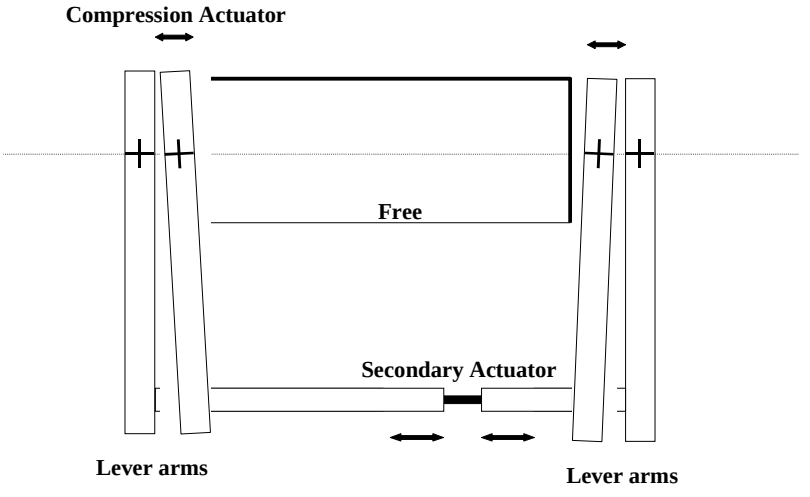

(c) Applying Strain Gradients

Figure 2: Unstiffened plate tests under constant strain eccentricity

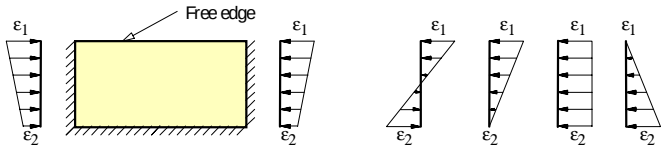

Figure 3: Strain gradients for test series

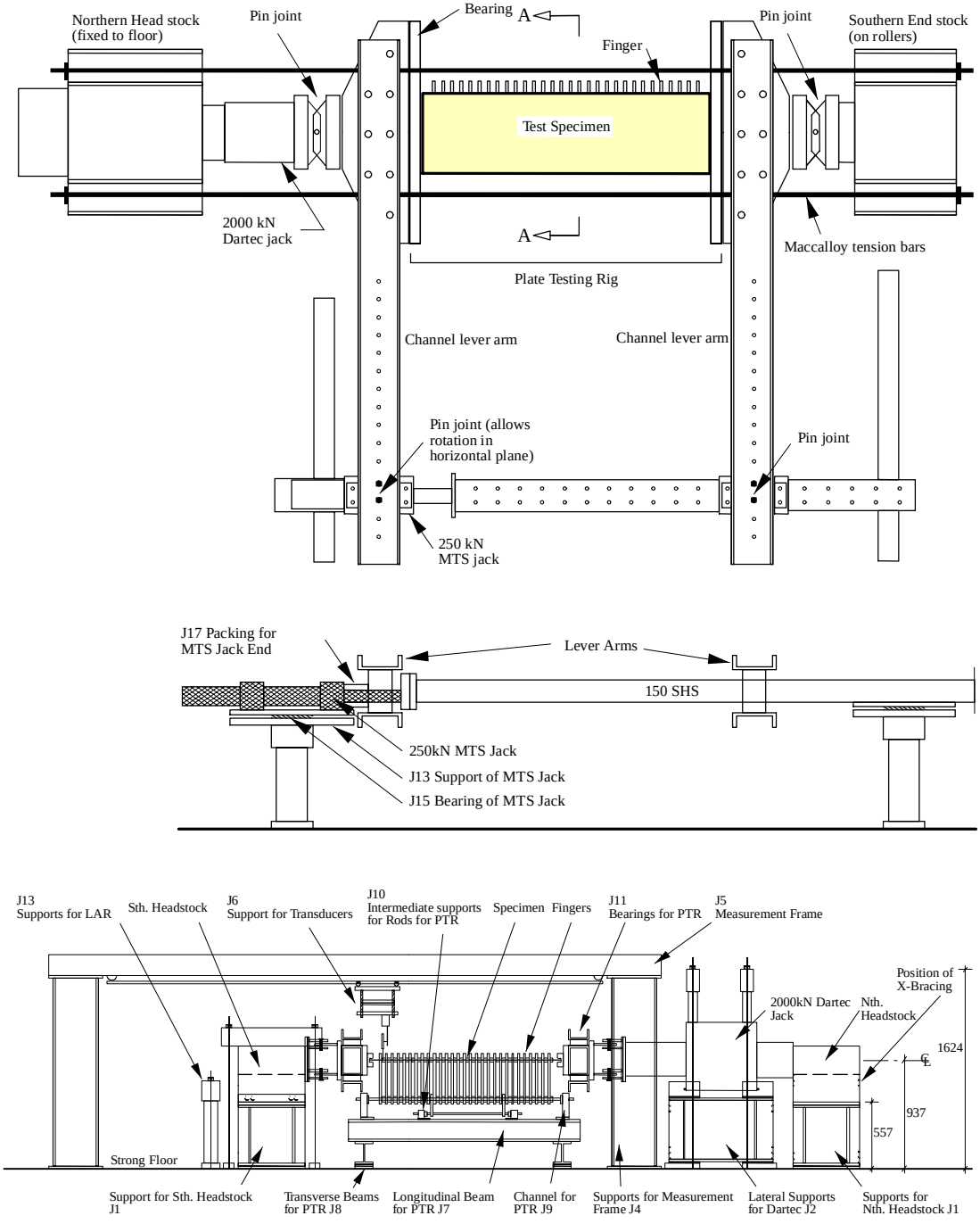

Figure 4: Plan and elevation of the dual actuator plate testing rig

(a) Overall view

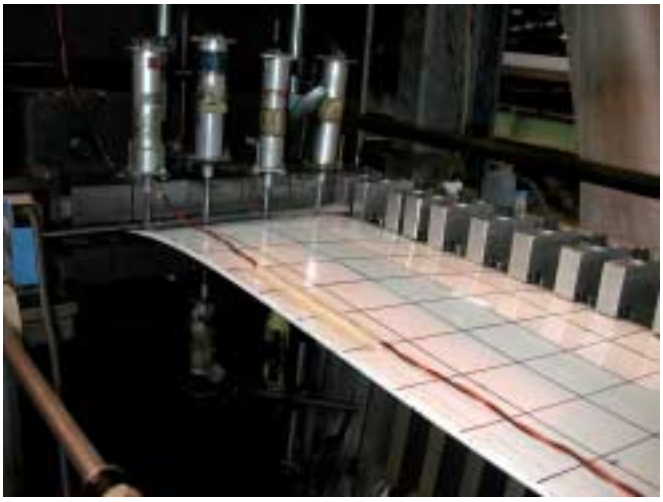

(b) Close-up view showing specimen and the lateral displacement measurement transducers

Figure 5: Photos of the dual actuator plate testing rig

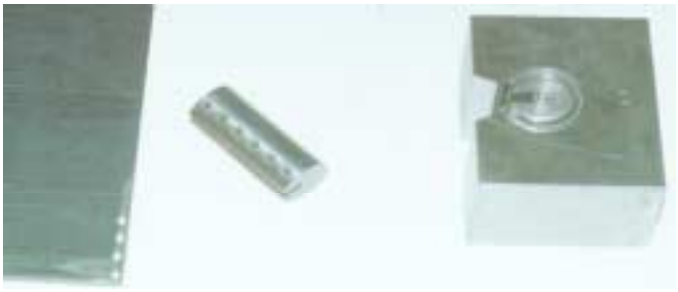

Figure 6: Loaded edge of a plate specimen, rod segment and end bearing

Figure 7: Discrete finger support

Figure 8: (a) End bearings and fingers provide three-sided simple support (b) Laser device and target

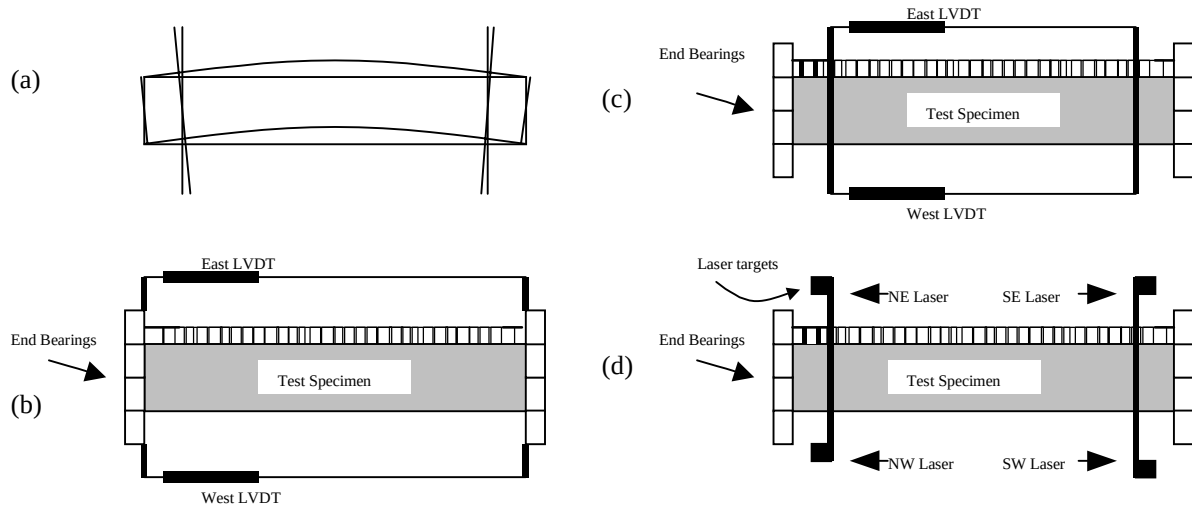

Figure 9: Independent displacement measurement systems

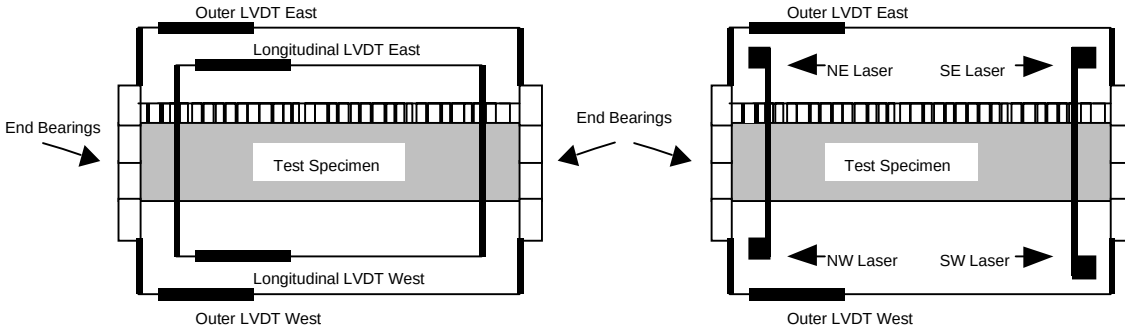

(a) Stocky specimens (b) Slender specimens

Figure 10: Independent displacement measurement systems used for the test series

Figure 11: Limit of end rotation due to contact of specimen and bearing block

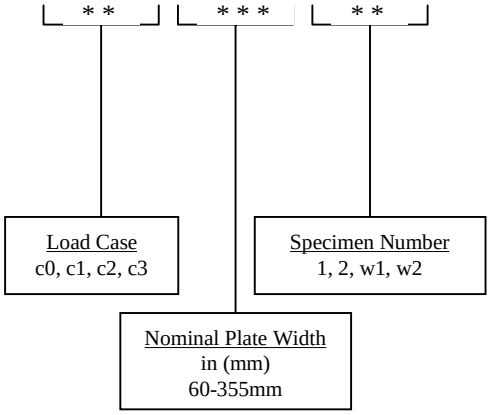

e.g. c0 80 w1

Load case: c0 (pure compression)
Nominal plate width: 80mm
Specimen number: Welded specimen #1

Figure 12: General specimen labeling system

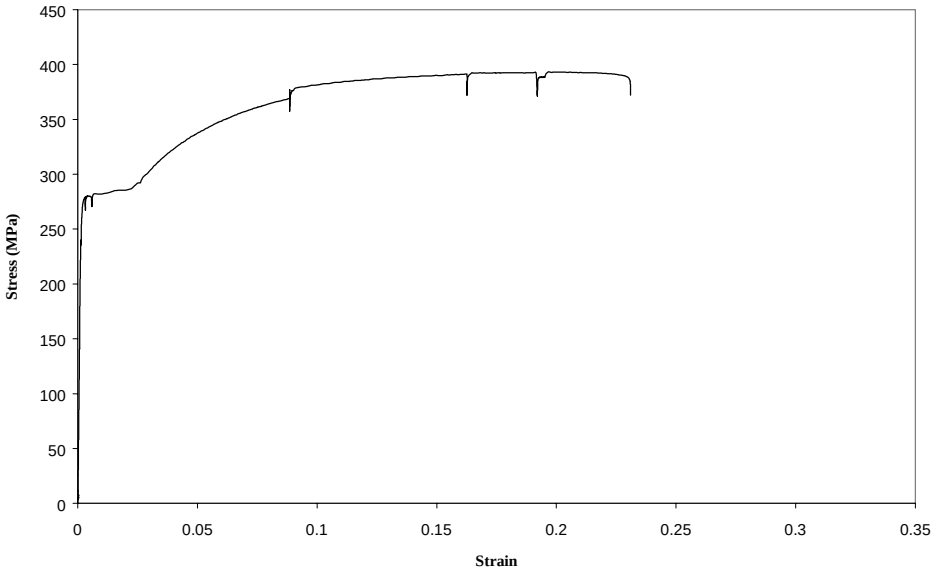

Figure 13: Complete stress-strain curve for Plate 1

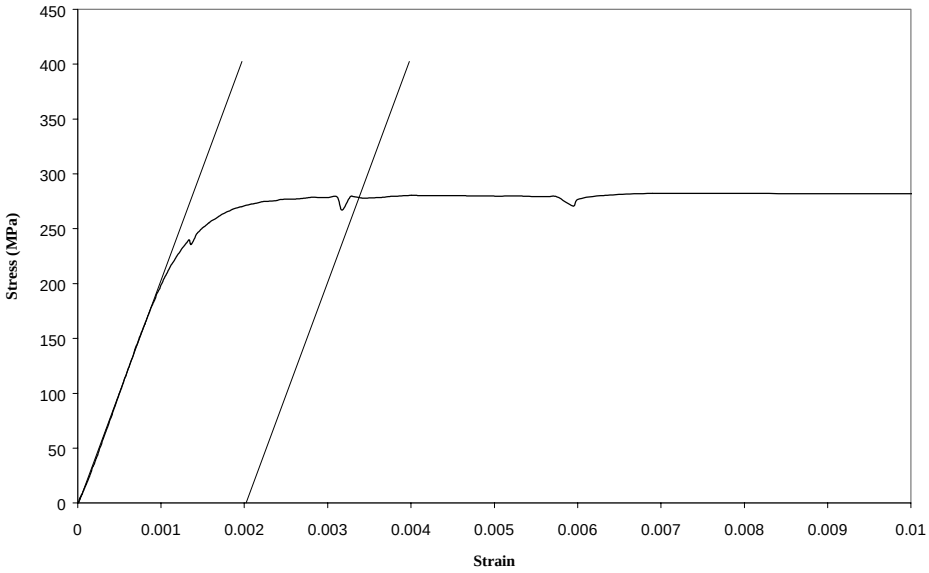

Figure 14: Initial part of stress-strain curve for Plate 1

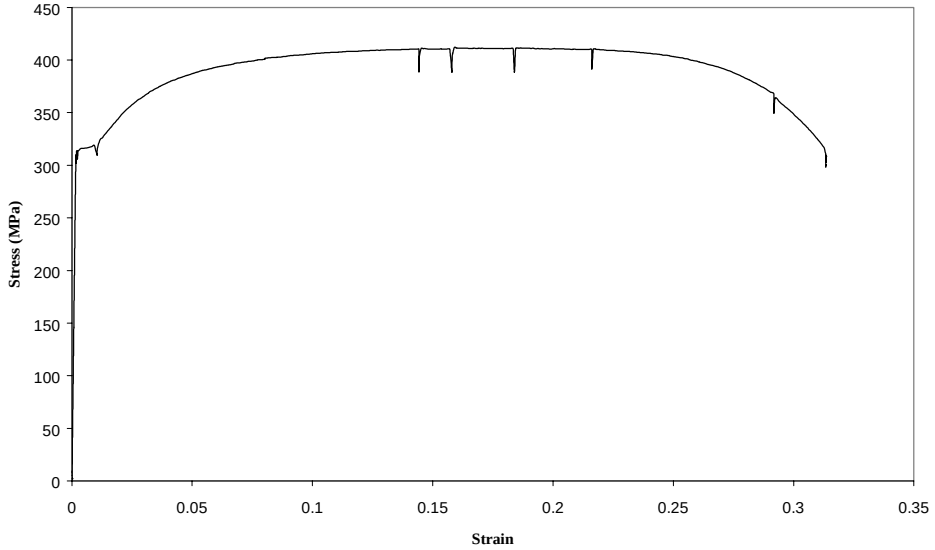

Figure 15: Complete stress-strain curve for Plate 2

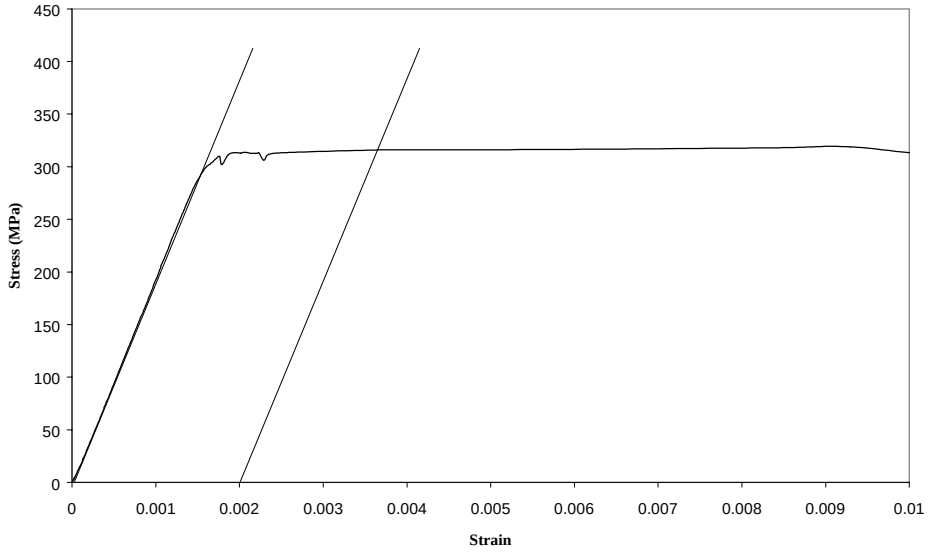

Figure 16: Initial part of stress-strain curve for Plate 2

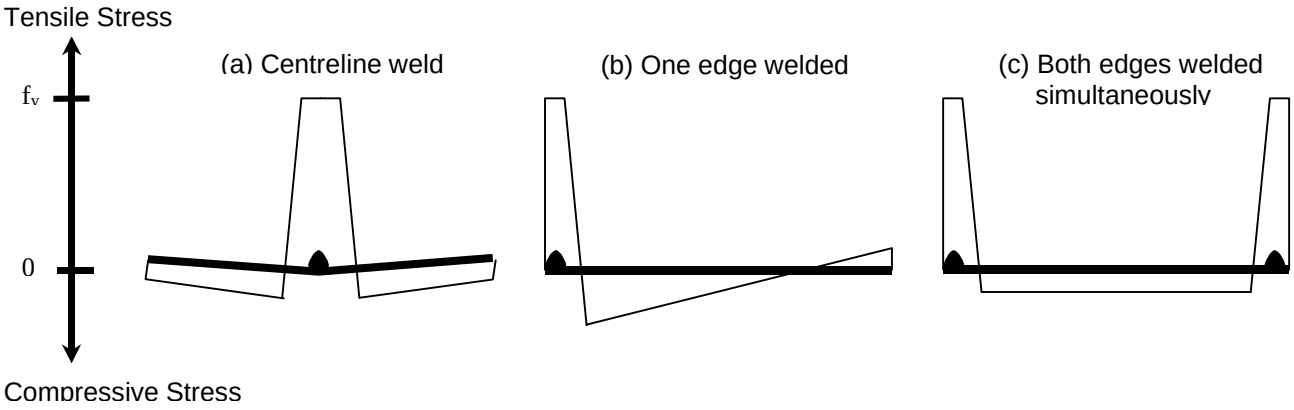

Figure 17: Residual Stress Profiles for Bead-on-Thin-Plate Welds

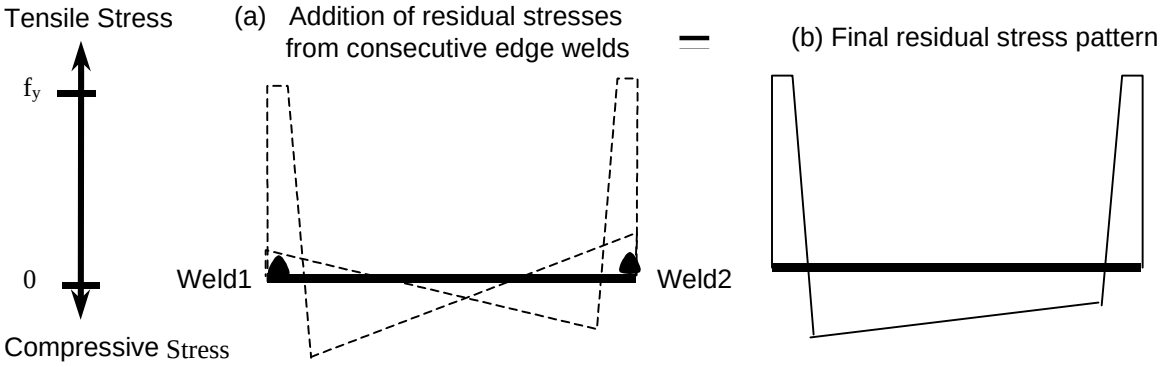

Figure 18: Addition of Residual Stresses from Consecutive Edge Welds

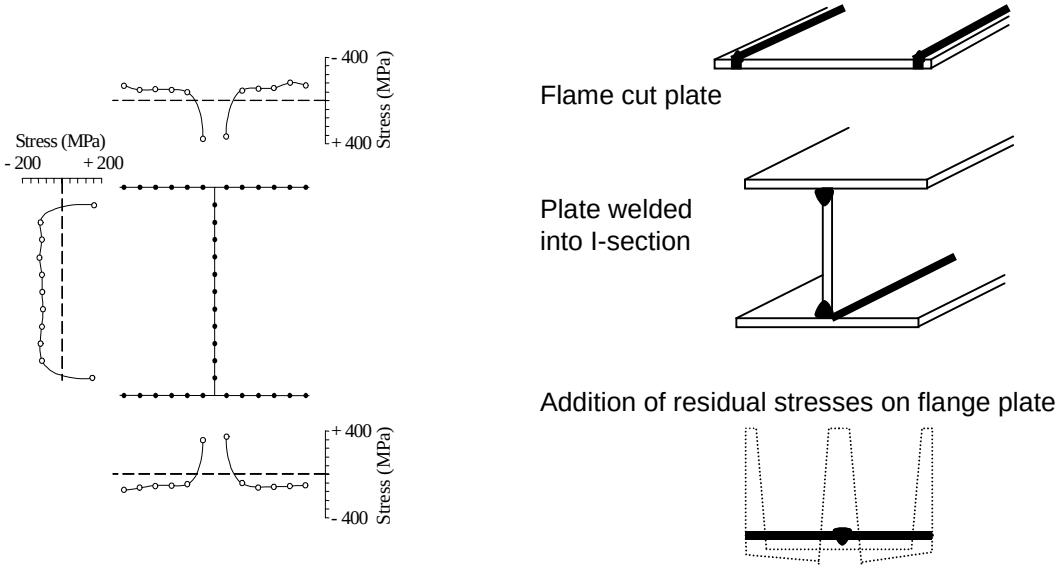

(a) I-section fabricated from stress free plates (b) I-section fabricated from flame cut plates

Figure 19: Residual Stress Profiles in Fabricated I-Sections

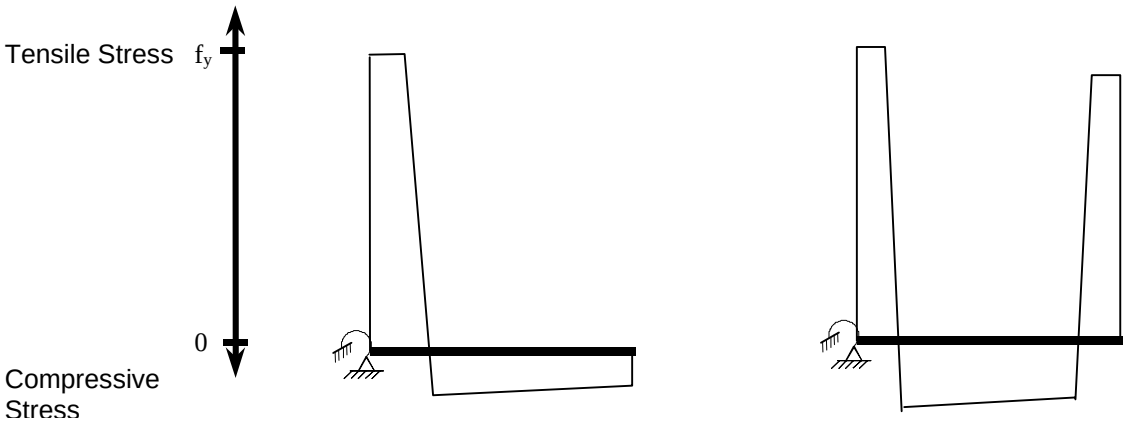

(a) I-section fabricated from stress free plates (b) I-section fabricated from flame cut plates

Figure 20: Residual Stress Profiles in Flange Outstands of Fabricated I-Sections

Figure 21: Welding Table Setup

Figure 22: Extensometer to record welding residual strains

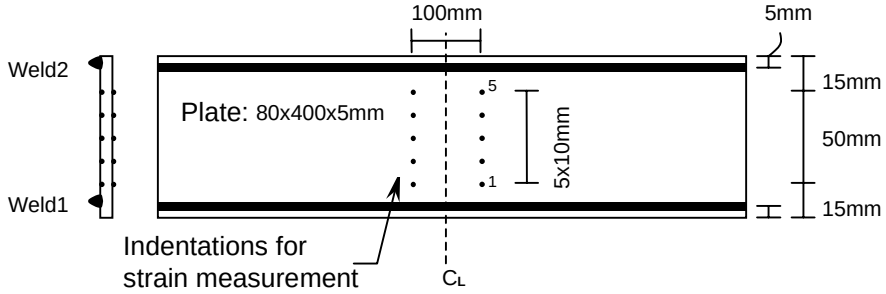

Figure 23: Typical Indentation Layout

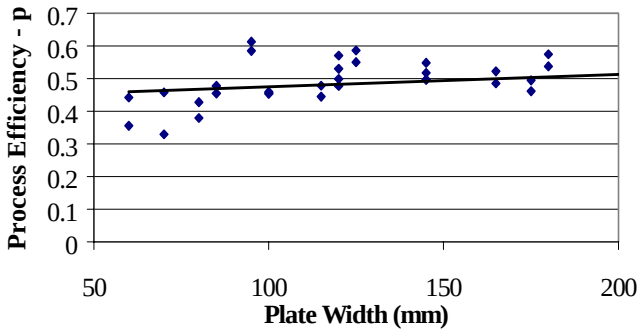

Figure 24: Process Efficiency vs Plate Width

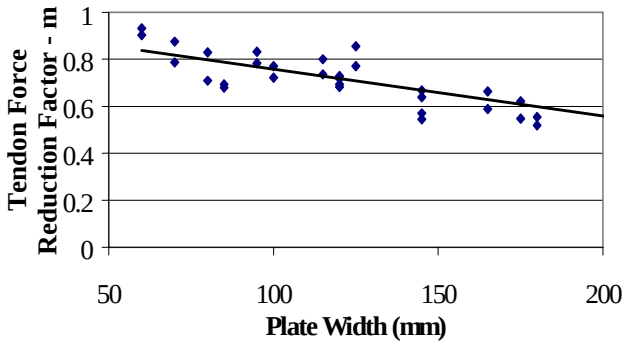

Figure 25: Reduction Factor vs Plate Width

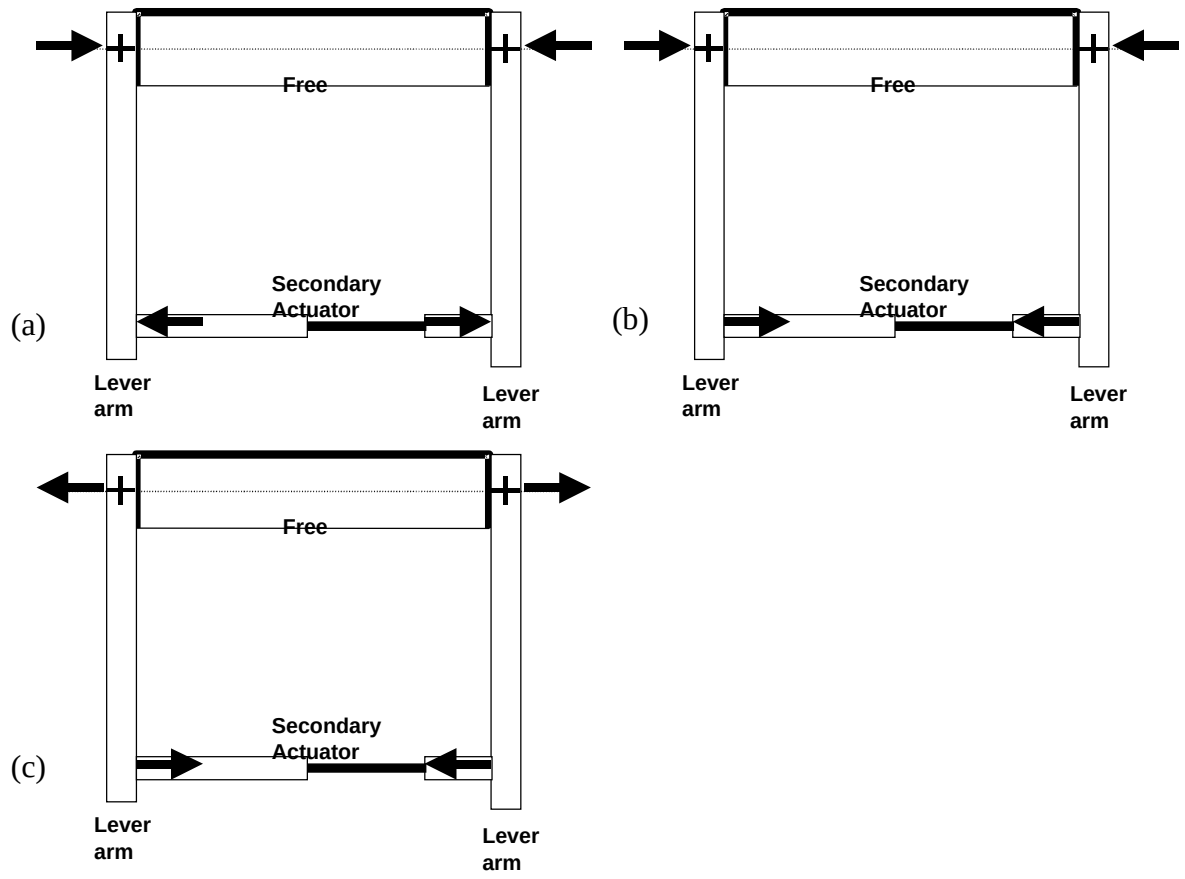

Figure 26: Directions of applied forces from the primary and secondary actuators

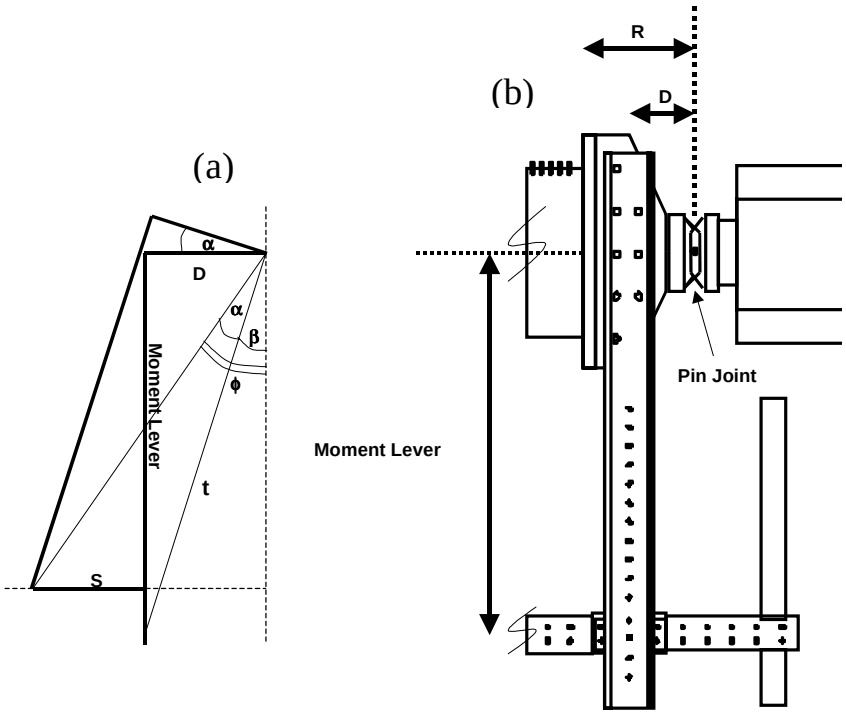

Figure 27: Calculation of the moment due to the eccentricity of the centreline of the specimen to the centreline of the primary actuator

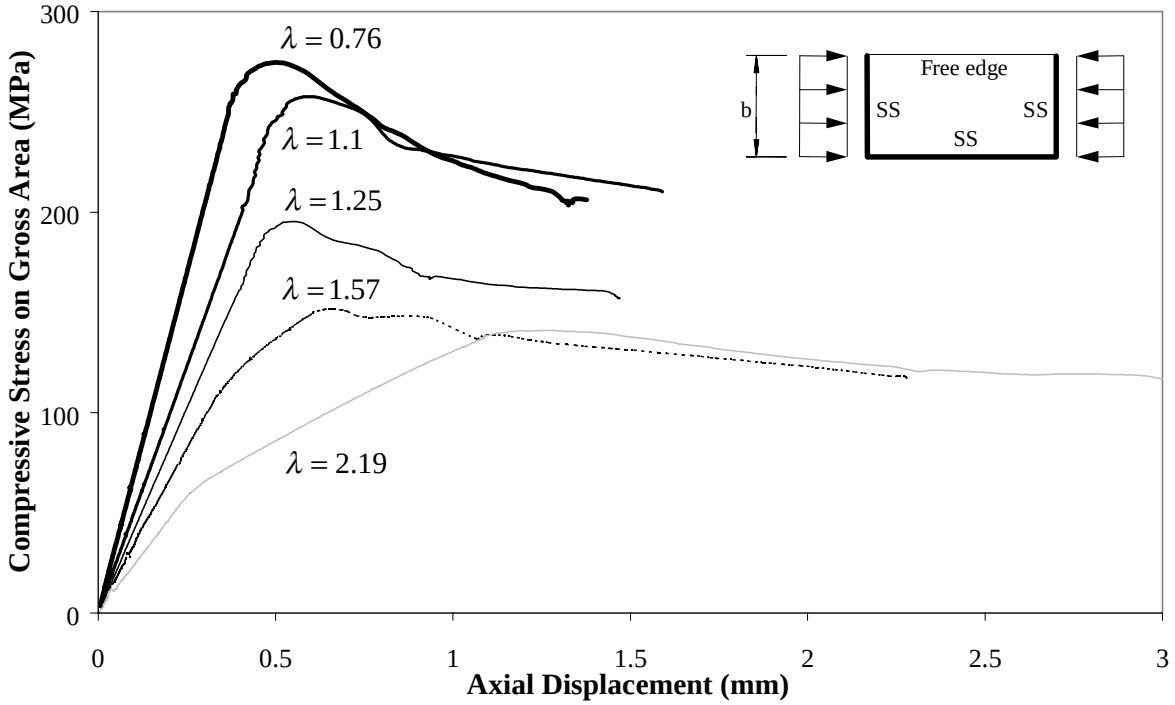

Figure 28: Pure compression plate test results for various slenderness rations - Unwelded specimens

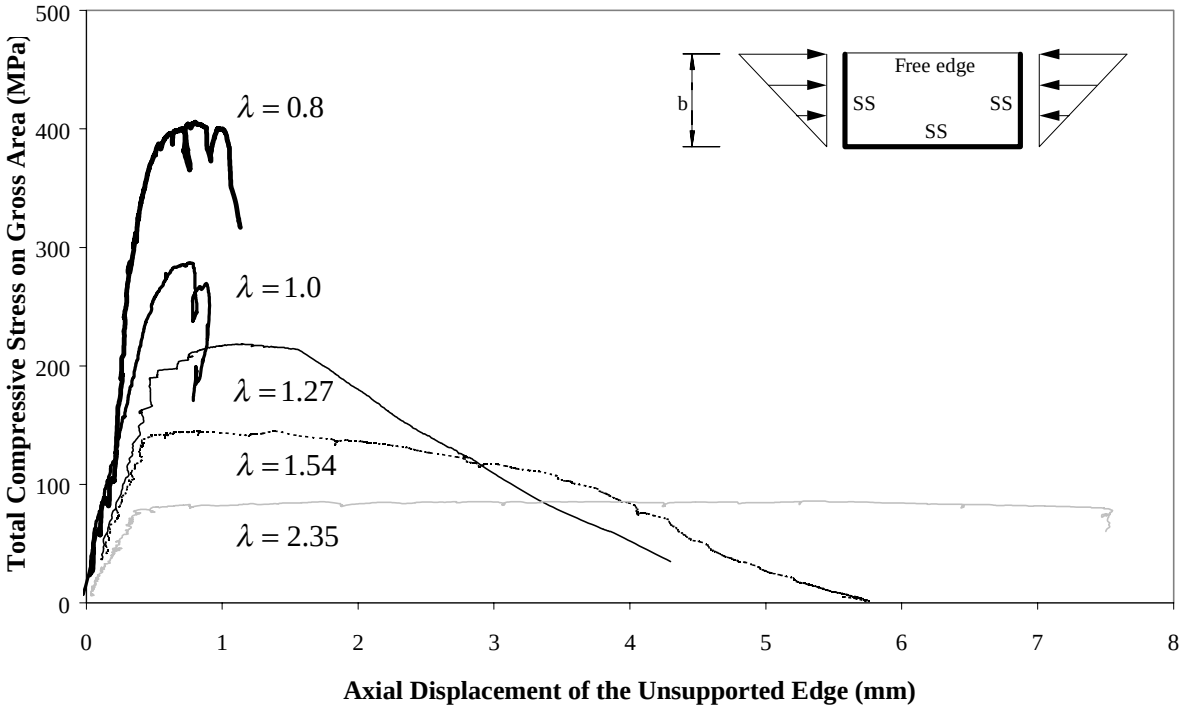

Figure 29: Compression at unsupported edge, zero at supported edge plate test results for various slenderness rations - Unwelded specimens

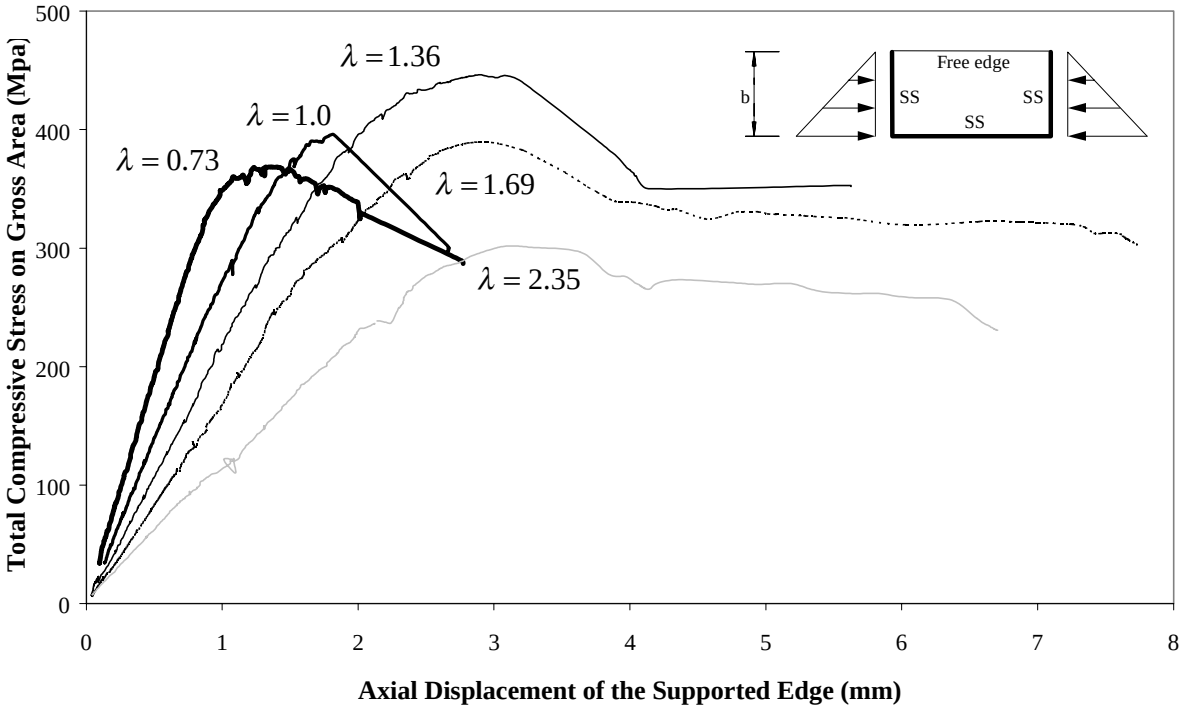

Figure 30: Compression at supported edge, zero at unsupported edge plate test results for various slenderness rations - Unwelded specimens

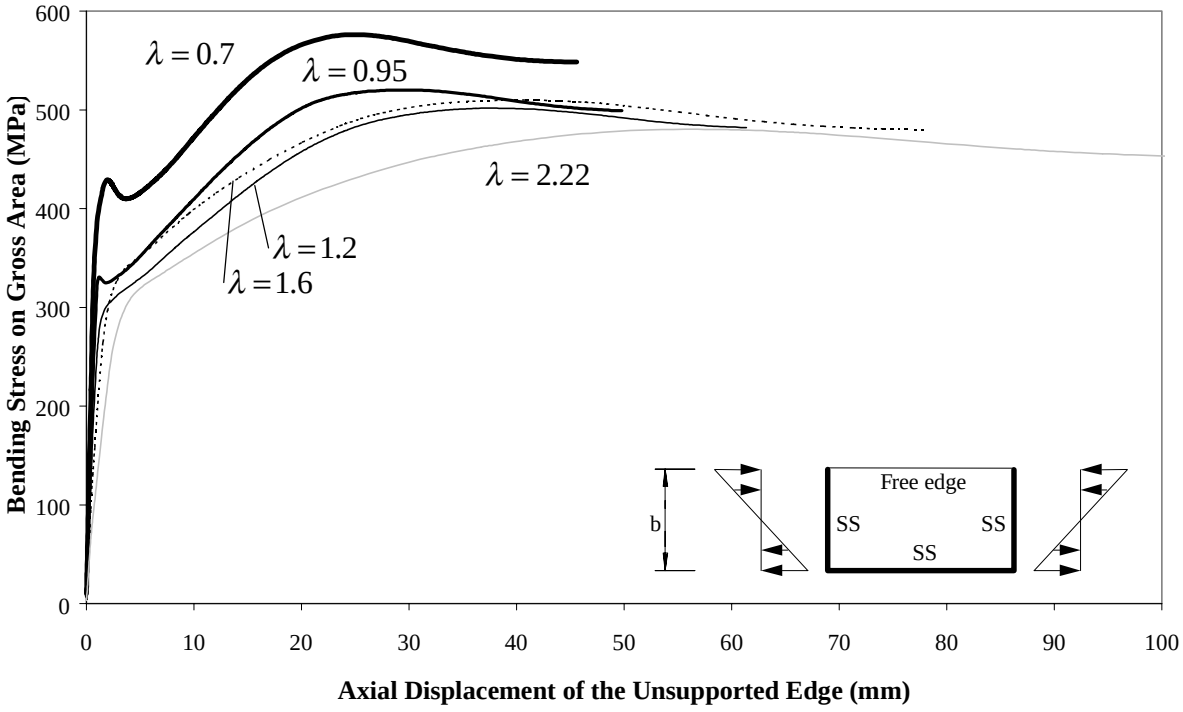

Figure 31: Pure bending Abaqus results for various slenderness rations - Unwelded specimens

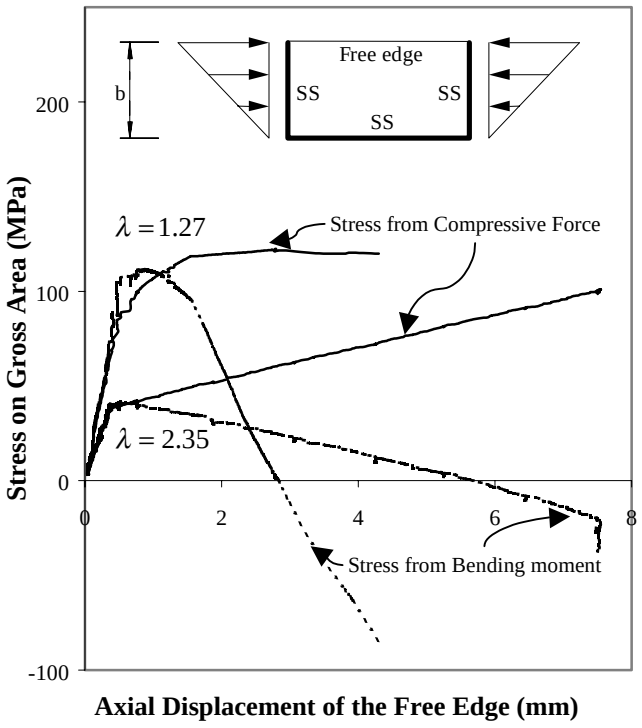

Figure 32: Compression at unsupported edge, zero at supported edge plate test results for various slenderness ratios – Unwelded specimens

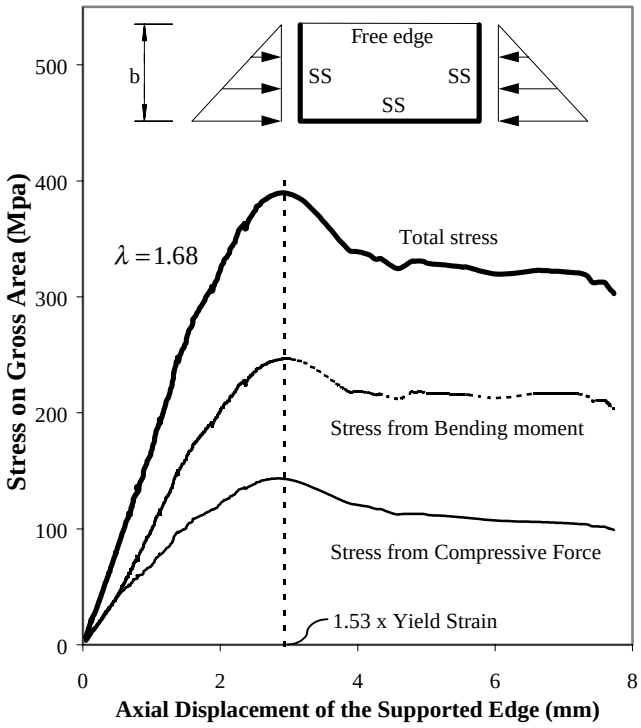

Figure 34: Compression at the supported edge, zero at the unsupported edge, Unwelded plate test result

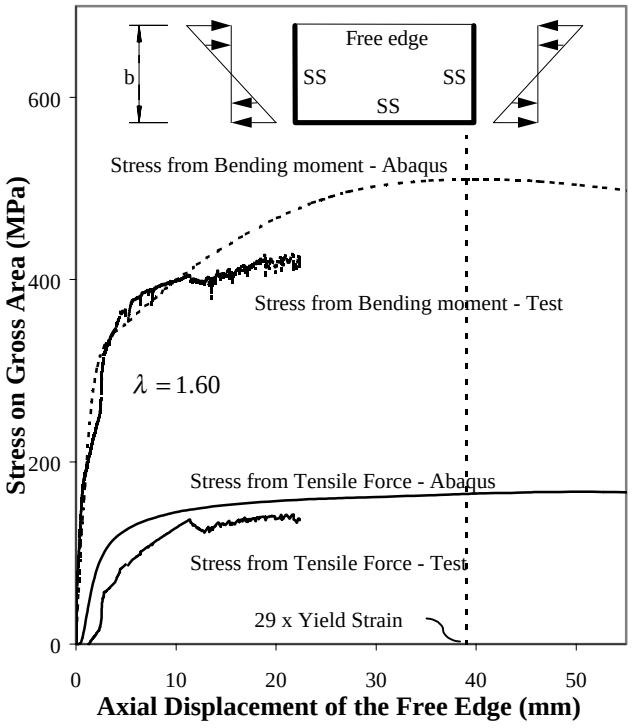

Figure 33: Pure bending with compression at the unsupported edge, Unwelded plate test and Abaqus comparison

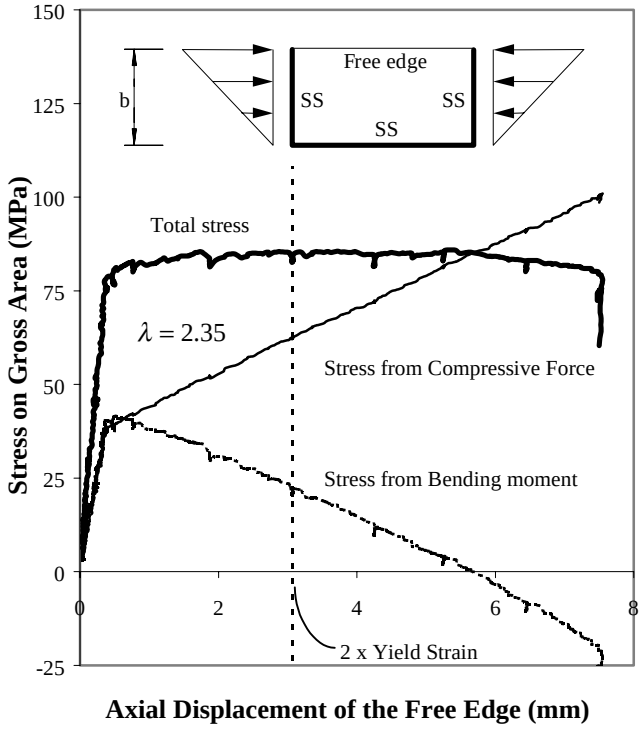

Figure 35: Compression at the unsupported edge, zero at the supported edge, Unwelded plate test result